Male mammalian meiosis and spermiogenesis is critically dependent on the shared functions of the katanins KATNA1 and KATNAL1

Authors

Jessica EM Dunleavy[1], Maddison Graffeo[1], Kathryn Wozniak[2], Anne E O'Connor[1], D. Jo Merriner[1], Joseph Nguyen[1], Ralf B Schittenhelm[3], Brendan J Houston[1], Moira K O'Bryan[1]

[1]School of BioSciences and Bio21 Institute, Faculty of Science, The University of Melbourne, VIC, 3010, Australia. [2]Monash Biomedicine Discovery Institute and The Department of Anatomy and Developmental Biology, Monash University, Melbourne VIC, 3800, Australia [3]Monash Proteomics & Metabolomics Facility, Department of Biochemistry and Molecular Biology, Biomedicine Discovery Institute, Monash University, Clayton VIC, 3800, Australia

***Correspondence:** Jessica.dunleavy@unimelb.edu.au

Summary

Katanin microtubule severing enzymes are potent M-phase regulators in oocytes and somatic cells. How the complex, and evolutionarily critical, male mammalian meiotic spindle is sculpted remains unknown. Here, using multiple single and double gene knockout mice, we reveal that the canonical katanin A-subunit, KATNA1, and its close paralogue, KATNAL1, together execute multiple aspects of meiosis. We show KATNA1 and KATNAL1 collectively regulate the male meiotic spindle, cytokinesis and midbody abscission, in addition to diverse spermatid remodelling events, including Golgi organisation, and acrosome and manchette formation. We also define KATNAL1-specific roles in sperm flagella development, manchette regulation, and sperm-epithelial disengagement. Finally, using proteomic approaches we define the KATNA1, KATNAL1, and KATNB1 mammalian testis interactome, which includes a network of cytoskeletal and vesicle trafficking proteins. Collectively, we reveal the presence of multiple katanin A-subunit paralogs in mammalian spermatogenesis allows for 'customized cutting' via neofunctionalization and protective buffering via gene redundancy.

Keywords: Meiotic spindle, spermatogenesis, microtubule severing, manchette, axoneme, acrosome, HTCA, male fertility, vesicle transport, spermiation

Introduction

The katanins are an evolutionary conserved family of microtubule (MT) severing proteins that were first identified as an essential meiosis regulator in *Caenorhabditis elegans* oocytes[1]. Since then, they have been established as a nuanced regulator of MTs, able to employ the same action (physical removal of tubulin heterodimers from the MT lattice) to amplify, disassemble or even strengthen MTs (for reviews see[2,3]). At a cellular level these actions drive rapid MT

39 remodelling events required in many processes including ciliogenesis, cell division and
40 differentiation, and allow fine tuning of homeostatic MT structures and processes.
41
42 The canonical katanin complex consists of an AAA ATPase catalytic severing enzyme
43 KATNA1 (aka p60 or A-subunit) and a WD40-repeat containing regulatory subunit KATNB1
44 (aka p80 or B-subunit) and is conserved across most eukaryotes. In its active ATP bound state,
45 the A-subunit forms a spiral hexamer which binds MTs and threads the C-terminal tail (CTT)
46 of a tubulin subunit through its central pore. An ATP-driven conformational change in the
47 hexamer, causes an extractive force on the tubulin CTT removing the tubulin heterodimer from
48 the lattice. In higher eukaryotes, the B-subunit is not essential for A-subunit severing activity,
49 however it increases MT affinity and severing efficiency, and at a cellular level is often
50 essential for A-subunit localisation[2]. In vertebrates, *Drosophila,* and unicellular ciliates,
51 paralogous A-subunits, KATNAL1 and KATNAL2 are present, and an additional WD40-less
52 KATNB1 paralog, KATNBL1 is present in vertebrates. KATNAL1 is highly similar in
53 sequence and domain architecture to KATNA1[2] and has been shown to possess MT-severing
54 activity[4]. KATNAL2 however, outside of the conserved AAA ATPase MT severing domain,
55 differs in domain architecture to KATNA1 and KATNAL1[2] and in standard MT severing
56 assays did not exhibit MT severing activity[4,5]. This aside, loss of KATNAL2 function in mouse
57 spermatogenesis resulted in phenotypes consistent with loss of MT severing[5].
58
59 Across eukaryotes, the regulation of cell division is a defining feature of katanin action. In *C.*
60 *elegans* oocytes, the orthologues of KATNA1 and KATNB1, MEI-1 and MEI-2 drive
61 formation of the bipolar spindle in meiosis I via MT amplification, and subsequently regulate
62 spindle length, function and positioning[2,6] and in meiosis II, mediate spindle disassembly[7].
63 KATNA1 has also been shown to regulate female meiotic spindle length in *Xenopus laevis* and

64 *Xenopus tropocalis*[8], and in cultured mouse oocytes KATNAL1 depletion results in abnormally
65 long meiotic spindles and an increase in multipolar spindles [9]. Likewise, in mitosis, katanin
66 A-subunits have variously been shown to regulate mitotic spindle size/shape, polarity, density
67 and orientation, and drive midbody abscission during cytokinesis in species ranging from
68 unicellular ciliates and plants to mammalian cell lines[2,6,10]. Despite these data, the contribution
69 of katanin proteins to male meiosis has received little attention. The requirement, and identity,
70 of katanin A-subunits in male mammalian meiosis has not been directly tested, although data
71 from loss-of-functions in the regulatory, B-subunit, KATNB1, strongly suggest katanin-
72 mediated MT severing is required[11,12].
73
74 Herein we aimed to identify the function of katanin-A subunits in male mammalian meiosis.
75 Using a suite of single and double katanin A-subunit deletion mice, we reveal KATNA1 and
76 KATNAL1 collectively regulate male meiosis, wherein they refine metaphase spindle structure
77 and chromosome alignment and drive accurate chromosome segregation. We show their
78 functions extend into haploid germ cell development (spermiogenesis), a process that
79 necessitates the development of several specialised MT structures. We identify KATNA1 and
80 KATNAL1 as global regulators of spermatid MTs required to restrain MT bulk, and as well as
81 identifying several structure/process specific roles, including in Golgi function and acrosome
82 biogenesis. We further identify KATNAL1 specific roles in cytokinesis during meiosis, in the
83 formation of the sperm head-to-tail coupling apparatus (HTCA) and axoneme, in sperm head
84 sharping via manchette MT dynamics and dissolution, and in sperm release (spermiation).
85 During spermatogenesis, we reveal KATNAL1 can fully functionally compensate for loss of
86 KATNA1. In contrast, we show KATNA1 can only partially compensate for KATNAL1 loss,
87 and there is no functional compensation between KATNA1 and KATNAL2 in the mouse testis.
88 Finally, using an *in vivo* immunoprecipitation (IP)-mass spectrometry (MS) approach, we

89 reveal these diverse cellular functions are mediated by an equally diverse set of KATNA1,
90 KATNAL1 and KATNB1 testis interacting partners, including MT associated proteins,
91 regulators of actin dynamics and organisation, vesicle-transport proteins including multiple
92 Rab GTPase family members, and essential mediators of male meiosis and acrosome
93 biogenesis. Collectively these results reveal the complex reliance of spermatogenesis on
94 katanin function and the precise neofunctionalization of A-subunits required to achieve normal
95 sperm function and morphology.
96
97 **Results**
98 **KATNA1 is not essential for male fertility in the mouse**
99 Despite the clear necessity for the dynamic regulation of MT structures during meiosis, and
100 data showing that the loss of the KATNB1 leads to notable defects in meiosis[11,12], the 'effector'
101 A-subunit is unknown. Data from *C. elegans* reveal the KATNA1 orthologue MEI-1 is a key
102 regulator of female meiosis. To test the hypothesis that KATNA1 serves an analogous function
103 in male meiosis, we generated a *Katna1* germ cell specific knockout mouse model
104 (*Katna1*$^{GCKO/GCKO}$, Fig S1A-C). As shown in Fig S1D, *Katna1* mRNA expression was reduced
105 by 91.77% in *Katna1*$^{GCKO/GCKO}$ spermatocytes compared to *Katnal1*$^{Flox/Flox}$ controls. Loss of
106 KATNA1 at the protein level was confirmed via immunolabelling of testis sections (Fig S1E).
107
108 *Katna1*$^{GCKO/GCKO}$ mice had normal body weight (Fig S2A) and unexpectedly were fertile.
109 *Katna1*$^{GCKO/GCKO}$ mice exhibited normal testis weight, testis daily sperm production and
110 epididymal sperm content (Fig S2B,C,D). Histological assessment of the male reproductive
111 tract in *Katna1*$^{GCKO/GCKO}$ mice revealed normal progression of germ cells through all phases of
112 spermatogenesis and the presence of sperm in the epididymis (Fig S2E,F,G). Sperm from
113 *Katna1*$^{GCKO/GCKO}$ mice were cytologically comparable to those from *Katnal1*$^{Flox/Flox}$ controls

114 (Fig S2H) and were functionally competent, as exhibited by normal fertility when mated with
115 wild-type females (8.2 pups per copulatory plug in *Katna1*$^{GCKO/GCKO}$ versus 7.1 pups in
116 controls, P=0.0969). Collectively, these data reveal KATNA1 is dispensable for mammalian
117 spermatogenesis.
118
119 **Germ cell derived KATNAL1 is required for optimal male fertility in mice**
120 We next sought to explore the requirement in meiosis for the non-canonical katanin A-subunit,
121 KATNAL1. A role for KATNAL1 in the somatic Sertoli cell population of the testis has been
122 defined [13], but a specific role in male meiosis has not been tested. To do this we generated a
123 *Katnal1* germ cell specific knockout mouse model (*Katnal1*$^{GCKO/GCKO}$, Fig S3A,B). Successful
124 ablation of *Katnal1* gene expression was confirmed by qPCR, western blotting of purified germ
125 cells and immunolabeling of testis sections (Fig 3C-E). There was a 99.56% reduction in
126 *Katnal1* mRNA in *Katnal1*$^{GCKO/GCKO}$ compared to *Katnal1*$^{Flox/Flox}$ germ cells.
127

128 *Katnal1*$^{GCKO/GCKO}$ males exhibited normal mating frequency but were subfertile siring 84%
129 fewer pups per copulatory plug than *Katnal1*$^{Flox/Flox}$ controls (6.9 ± 3.1SD pups / plug sired by
130 *Katnal1*$^{Flox/Flox}$ males versus 1.4 ± 1.6SD pups / plug sired by *Katnal1*$^{GCKO/GCKO}$ males,
131 P=0.0151). As outlined below, this subfertility was due to a dramatic reduction in sperm
132 number, and abnormal sperm morphology and motility. *Katnal1*$^{GCKO/GCKO}$ mice had body and
133 testis weights comparable to *Katnal1*$^{Flox/Flox}$ mice (Fig 1A,B). Likewise, the number of
134 apoptotic germ cells per seminiferous tubules was not significantly different between
135 *Katnal1*$^{Flox/Flox}$ and *Katnal1*$^{GCKO/GCKO}$ mice (Fig 1D). Despite this, *Katnal1*$^{GCKO/GCKO}$ testis
136 daily sperm production was reduced by 42.3% compared to *Katnal1*$^{Flox/Flox}$ mice (Fig 1C),
137 indicative of germ cell loss in the later steps of spermiogenesis, when spermatids contribute
138 minimally to the overall weight of the testis. Finally, epididymal sperm content was reduced

139 by 73.7% compared to *Katnal1*$^{Flox/Flox}$ mice (Fig 1D). This reveals that germ cell derived
140 KATNAL1 is required for optimal spermiogenesis and, as evidenced by the more severe
141 reduction in epididymal sperm content relative to DSPs, for their ultimate release from the
142 seminiferous epithelium via the process of spermiation. Assessment of *Katnal1*$^{GCKO/GCKO}$
143 seminiferous tubule histology confirmed the abnormal retention of elongated spermatids in
144 stage IX tubules (Fig 1G).

145

146 While all germ cell types were present in the *Katnal1*$^{GCKO/GCKO}$ seminiferous epithelium, many
147 *Katnal1*$^{GCKO/GCKO}$ tubules contained fewer germ cells, notably spermatids, compared to
148 *Katnal1*$^{Flox/Flox}$ mice (Fig 1E,F). Areas of Sertoli cell-only tubules were observed and gaps
149 between adjacent Sertoli cells were frequently seen in *Katnal1*$^{GCKO/GCKO}$ but never in
150 *Katnal1*$^{Flox/Flox}$ (Fig 1E,F). Epididymal histology was consistent with the presence of fewer
151 sperm in *Katnal1*$^{GCKO/GCKO}$, in addition to the presence of prematurely sloughed germ cells in
152 *Katnal1*$^{GCKO/GCKO}$, but not *Katnal1*$^{Flox/Flox}$, mice (Fig 1H). Of note, immunolabelling testis
153 sections for the Sertoli cells specific β-tubulin isoform, TUBB3, confirmed the origins of the
154 reduced spermatogenic output in the *Katnal1*$^{GCKO/GCKO}$ were distinct from those of the
155 previously characterised *Katnal1*$^{1H/1H}$ hypomorphic mouse model where extensive disruption
156 of the Sertoli cell MT cytoskeleton was seen [13]. In contrast, in *Katnal1*$^{GCKO/GCKO}$ testis sections
157 TUBB3 localisation was comparable to *Katnal1*$^{Flox/Flox}$ (Fig S4A-B). These data reveal that
158 KATNAL1 plays an essential role in the regulation of MTs in both Sertoli and germ cells.

159

160 Of the sperm present in the epididymides of *Katnal1*$^{GCKO/GCKO}$ mice, almost all were
161 morphologically abnormal (97.1% in *Katnal1*$^{GCKO/GCKO}$ versus 23.9% in *Katnal1*$^{Flox/Flox}$, Fig
162 1I,J). Abnormalities included in head shape (97.1% in *Katnal1*$^{GCKO/GCKO}$ versus 11.3% in

163 *Katnal1*$^{Flox/Flox}$), head position (36.4% versus 2.3%), coupling between the head and tail
164 (decapitation, 34.7% versus 11.5%), mid-pieces structure (coiling, 14.4% versus 0.0%) and
165 mitochondrial sheath structure (3.9% versus 0.0%) (Fig 1J). Moreover, of those sperm found
166 in *Katnal1*$^{GCKO/GCKO}$ epididymides, there was a 20.2% reduction in the ability for motility and
167 a 52.9% reduction in progressive motility in the absence versus presence of KATNAL1 (Fig
168 2K,L). Considering the reduction in sperm number in *Katnal1*$^{GCKO/GCKO}$ mice, this equates to
169 an 87.6% reduction in the total number of progressively motile sperm in *Katnal1*$^{GCKO/GCKO}$
170 compared to *Katnal1*$^{Flox/Flox}$ mice. Collectively these phenotypes reveal germ cell derived
171 KATNAL1 is required for normal spermatogenesis and optimal male fertility.
172
173 **KATNAL1 regulates chromosome alignment, segregation and cytokinesis during male**
174 **meiosis**
175 The reduction in post-meiotic germ cells in *Katnal1*$^{GCKO/GCKO}$ seminiferous tubules indicated a
176 variably penetrant meiotic defect. To assess *Katnal1*$^{GCKO/GCKO}$ meiotic spindles, testis sections
177 were stained for α-tubulin as a component of MTs (Fig 2A,B). As seen in *Katnal1*$^{Flox/Flox}$ stage
178 XII tubules, metaphase I and II meiotic spindle MTs typically project from the two opposing
179 spindle poles in a narrow and uniform angle to tightly align chromosomes/chromatids along
180 the metaphase plate (Fig 2Aa,2Ba-c). In *Katnal1*$^{GCKO/GCKO}$ stage XII tubules, the vast majority
181 of metaphase spindles displayed normal spindle architecture and normal MT spindle density
182 (Fig 2Ae, Bf-h). Chromosomal alignment at the metaphase plate, however, was noticeably
183 abnormal in many *Katnal1*$^{GCKO/GCKO}$ metaphase spermatocytes, with misaligned chromosomes
184 often observed (Fig 2A,Bf-g, green arrowheads). These defects did not however prevent
185 progression to anaphase, with no increase in metaphase arrest and apoptosis in stage XII-I
186 seminiferous tubules in *Katnal1*$^{GCKO/GCKO}$ compared to *Katnal1*$^{Flox/Flox}$ mice (Fig 2A,E-J).
187

188 Similarly, KATNAL1 loss in germ cells did not prevent spermatocyte progression through
189 anaphase and telophase. Specifically there was no discernible increase in *Katnal1*$^{GCKO/GCKO}$
190 spermatocytes stalling in anaphase or telophase or undergoing apoptosis (Fig 2A,E-J). Instead,
191 anaphase and telophase defects in *Katnal1*$^{GCKO/GCKO}$ meiosis led to the production of abnormal
192 haploid germ cells. In anaphase I and II, spindle MTs undergo poleward shortening, allowing
193 them to pull chromosomes toward opposing poles in a coordinated manner, as observed in
194 *Katnal1*$^{Flox/Flox}$ anaphase spermatocytes (Fig 2Ab,Bd-e). In *Katnal1*$^{GCKO/GCKO}$ anaphase
195 spermatocytes however, uneven segregation of chromosomes was often observed, with lagging
196 chromosomes commonly seen (Fig 2Af, Bi-j, green arrowheads). Consistent with uneven
197 chromosome segregation in anaphase, many round spermatids possessed abnormally large
198 nuclei (Fig 2Cb-c, yellow arrowheads). During telophase and cytokinesis midbodies were
199 present in *Katnal1*$^{GCKO/GCKO}$ and were comparable to those in *Katnal1*$^{Flox/Flox}$ spermatocytes
200 (Fig 2Ac,g). However, a subset of the resulting spermatids was binucleated (Fig 2Cd,e, orange
201 arrowheads), and as detailed below sperm/spermatids with multiple axonemes (Fig 3C) and
202 supernumerary centrioles (Fig 3Db, red arrowhead) were often observed. This indicates that
203 while midbodies do form in the absence of *Katnal1*, KATNAL1 plays a key role its remodelling
204 into an intracytoplasmic bridge and the maintenance of individual daughter spermatids.
205 Binucleated spermatids were never observed in *Katnal1*$^{Flox/Flox}$ tubules.
206
207 These data reveal KATNAL1 regulates MT-chromosome attachment and/or metaphase spindle
208 dynamics but is dispensable for MT generation and pruning during spindle biogenesis in male
209 meiosis. Moreover, our data show KATNAL1 greatly facilitates accurate chromosome
210 segregation during anaphase and midbody function and disassembly during cytokinesis in
211 either meiosis I and/or meiosis II.
212

213 **KATNAL1 regulates flagella and manchette formation in male germ cells**

214 As detailed above, of the epididymal sperm that were produced in *Katnal1*$^{GCKO/GCKO}$ mice
215 97.1% were morphologically abnormal revealing that KATNAL1 is required during spermatid
216 differentiation (spermiogenesis) (Fig 1I,J). One of the first processes to commence in
217 spermiogenesis is acrosome formation, and our recent data identified MT severing as a
218 potential regulator of this process [11]. The identity of the involved MT severing A-subunit
219 remains unknown. Acrosome formation was overtly normal in *Katnal1*$^{GCKO/GCKO}$ mice
220 compared to *Katnal1*$^{Flox/Flox}$ controls, indicating KATNAL1 is not essential for this process
221 (Fig S4C).

222

223 Multiple abnormalities were however observed in *Katnal1*$^{GCKO/GCKO}$ mouse sperm tails and the
224 head-to-tail coupling apparatus (HTCA), including abnormal reticulation of the sperm head,
225 decapitation, coiling of the sperm tail mid-piece and mitochondrial sheath defects, in addition
226 to reduced sperm motility. Staining of *Katnal1*$^{GCKO/GCKO}$ testis sections for acetylated tubulin,
227 as a marker of stable MTs, revealed axonemal MTs were present in sperm tails (Fig 3B),
228 however analysis via transmission electron microscopy (TEM) revealed a range of axoneme
229 and accessory structure abnormalities (Fig 3C). In *Katnal1*$^{GCKO/GCKO}$ mice, sperm flagella
230 axonemes often lacked the typical 9+2 MT doublet arrangement observed in controls (Fig
231 3Ca,d,g). Instead MT doublets were often missing (Fig 3Ce,f,h, yellow asterisks), ectopically
232 located (Fig 3C, red arrowheads) or in many cases supernumerary MT doublets were present
233 (Fig 3Cc,l, white arrowheads). In the most dramatic instances, and consistent with the failures
234 in cytokinesis, multiple axonemes, often each with associated accessory structures, were
235 observed within one cell (Fig 3Cb,j-l). The abnormalities in MT doublet number and location
236 were typically accompanied by defects in outer dense fiber (ODF) number and location (Fig
237 3C). In wild-type sperm, the mid-piece contains 9 ODFs closely associated with the 9 outer

238 MT doublets of the axoneme (Fig 3Ca). In the principal piece ODFs 3 and 8 are replaced by
239 the longitudinal columns of the fibrous sheath (Fig 3Cd). In *Katnal1*$^{GCKO/GCKO}$ mice however,
240 sperm tail ODFs 3 and/or 9 frequently persisted into the principal piece (Fig 3Cb,c, green
241 arrowheads). In *Katnal1*$^{GCKO/GCKO}$ mouse sperm tails wherein some or all axoneme MTs were
242 missing, ODFs were often also missing (Fig 3Ce,f). Consistent with the coiled mid-pieces and
243 mitochondrial sheath defects observed in some sperm from *Katnal1*$^{GCKO/GCKO}$ mice, TEM
244 revealed that in many sperm the mitochondria were not properly organised into a helical sheath
245 (Fig 3Cj). Fibrous sheath development in *Katnal1*$^{GCKO/GCKO}$ sperm however, appeared normal
246 in most cells (Fig 3C). Finally, in some sperm, only disorganised fragments of sperm tail
247 components were observed indicative of degenerating cells (Fig 3Cm). Collectively, these data
248 reveal KATNAL1-mediated MT severing regulates the assembly and potentially stability of
249 axoneme MT doublets, and that KATNAL1 contributes to the development of the
250 mitochondrial sheath and ODFs, but not the fibrous sheath. These data are consistent with
251 defects in cargo/organelle delivery to and along the growing sperm tail. Indeed, there is an
252 increasing of body of evidence (reviewed in[14]) that mitochondria and ODFs rely on MT-based
253 transport mechanisms for their delivery into the sperm tail.
254
255 The frequent decapitation or hyper-extension of sperm heads, in sperm from *Katnal1*$^{GCKO/GCKO}$
256 males, indicates the HTCA was weak and/or improperly formed in the absence of KATNAL1.
257 Moreover, TEM of round and elongated spermatids revealed a range of HTCA abnormalities
258 in *Katnal1*$^{GCKO/GCKO}$ mice compared to controls (Fig 3D). In *Katnal1*$^{Flox/Flox}$ mice, spermatid
259 HTCAs were easy to find in testis sections via TEM. As expected, they contained a proximal
260 centriole coupled to the nucleus via the basal plate and capitulum, a distal centriole coupled to
261 the plasma membrane and continuous with the axoneme, and the surrounding segmented
262 columns which are continuous with the ODFs (Fig 3Da,f). In *Katnal1*$^{GCKO/GCKO}$ mice, however

263 normal HTCAs were rare (Fig 3Db,g). In most spermatids, HTCAs were abnormal (Fig 3Dc-
264 e, h-j). In some cells, the HTCA and associated axoneme was present, but not attached to the
265 nucleus (Fig 3Dc,h, yellow arrowheads), while in others the basal plate could be seen
266 associated with the nucleus, but the rest of the HTCA was absent (Fig 3Dg). Consistent with
267 this data, immunolabelling of sperm for SUN5, which is an essential component of the LINC
268 complex that physically docks the sperm centrosome to the nucleus, revealed a 57.2%
269 reduction in sperm from *Katnal1*$^{GCKO/GCKO}$ males containing SUN5 at the HTCA compared to
270 sperm from *Katnal1*$^{Flox/Flox}$ mice (Fig S4D,E). These data suggest that KATNAL1 regulated-
271 MTs are either required to fortify the connection between the basal plate and the nucleus or are
272 required for the delivery and deposition of essential components of the HTCA. Our data also
273 suggest that SUN5 is delivered to the HTCA via KATNAL1-regulated MTs.
274
275 Abnormal head shape was the most frequent morphological abnormality present in the sperm
276 of *Katnal1*$^{GCKO/GCKO}$ mice. Instead of the normal hook shape exhibited in 88.75% of
277 *Katnal1*$^{Flox/Flox}$ mouse sperm, 34% of *Katnal1*$^{GCKO/GCKO}$ mouse sperm heads exhibited a
278 'hammerhead' shape and 62% exhibited a 'knobby' head phenotype (Fig 1I, S4F,G). Abnormal
279 head shaping became apparent during nuclear elongation (Fig 3E) and were consistent with
280 defects in manchette function, where the manchette is a transient MT-based structure which
281 sculpts the distal half of the spermatid head. As shown in Fig 3F in wild-type mice the
282 manchette forms in step 8-9 spermatids (stage VIII-IX seminiferous tubules), before migrating
283 distally while simultaneously constricting to shape the spermatids head during steps 10-12
284 (stages X-XII; Fig 3F). In steps 13-14 (stage I-III) the manchette is dissembled (Fig 4F). In
285 spermatids from *Katnal1*$^{GCKO/GCKO}$ mice, manchettes formed at step 8-9 but were abnormally
286 elongated. Elongation became increasingly pronounced as spermatid development continued
287 and was associated with a failure of manchette perinuclear ring migration down the sperm head,

288 but continued constriction, and resulting in a 'knobby head' phenotype (Fig 4G). Finally,
289 manchette disassembly in steps 13-14 was delayed in the absence of KATNAL1 (Fig 4F).
290 Collectively, these results reveal KATNAL1-mediated MT severing is required to regulate
291 manchette MT length, migration and disassembly.
292
293 **KATNA1 and KATNAL1 compensate for each other in male meiosis and spermiogenesis**
294 Given the apparently normal fertility in *Katna1*$^{GCKO/GCKO}$ and residual fertility in
295 *Katnal1*$^{GCKO/GCKO}$ mice, we sought to explore the possibility of functional compensation,
296 between KATNA1 and its paralogs KATNAL1 and KATNAL2 in the testis. This is a
297 particularly critical question for meiosis wherein the identity of the critical A-subunit(s)
298 remains unknown. As reported previously, *Katnal2* loss has no apparent effect on male meiosis
299 but does result in male infertility due to severe sperm developmental defects[5]. To test for
300 redundancy, we generated (1) *Katna1* and *Katnal1* double germ cell knockout mice
301 (*Katna1/al1*$^{GCKO/GCKO}$) and (2) double *Katna1* germ cell and *Katnal2* knockout mice
302 (*Katna1*$^{GCKO/GCKO}$*/al2*$^{KO/KO}$). The *Katna1*$^{GCKO/GCKO}$*/al2*$^{KO/KO}$ mouse model (Fig S5)
303 phenocopied our previously characterised *Katnal2* mutant models[5], including having a
304 comparable spermiation failure phenotype, sperm head shaping defects (knobby heads), and
305 an absence of normal sperm tail development (Fig S5). No aspect of the infertility phenotype
306 appeared worse that the loss of KATNAL2 in isolation. These data reveal that KATNA1 and
307 KATNAL2 do not have compensatory function in male germ cell development.
308
309 By contrast the removal of KATNA1 and KATNAL1 from germ cells resulted in a significantly
310 worse male fertility phenotype than seen in either individual knockout, especially in meiosis.
311 Successful ablation of both *Katna1* and *Katnal1* from male germ cells was confirmed by qPCR
312 (Fig 4A,B). Test mating of the *Katna1/al1*$^{GCKO/GCKO}$ male mice with wild-type females,

313 revealed loss of both KATNA1 and KATNAL1 from male germ cells results in male sterility
314 (7.1±3.2 SD pups / plug sired by *Katna1/al1*$^{Flox/Flox}$ males versus 0± 0 SD pups / plug sired by
315 *Katna1/al1*$^{GCKO/GCKO}$ males (P=0.0175)). Moreover, assessment of the reproductive tract
316 revealed a 48.5% reduction in testis weight, an 89% reduction in daily sperm output and a
317 96.2% reduction in epididymal sperm content compared to controls (Fig 4D-F). Examination
318 of *Katna1/al1*$^{GCKO/GCKO}$ seminiferous tubule histology instantly revealed large scale germ cell
319 loss during both meiosis and spermiogenesis that was significantly worse than in either single
320 gene deletion (Fig 4G-H). Numerous pyknotic spermatocytes were observed in all stage XII
321 and I *Katna1/al1*$^{GCKO/GCKO}$ tubules indicative of cells stalling in meiosis followed by apoptosis
322 but were rare in *Katna1/al1*$^{Flox/Flox}$ (Fig 4G-H, magenta arrowheads). Of the germ cells that
323 progressed through meiosis in *Katna1/al1*$^{GCKO/GCKO}$, the vast majority became pyknotic by
324 steps 12-13 (stages XII-I) of elongating spermatid development (Fig 4H, green arrowheads)
325 and as a result elongated spermatids were absent past stage II-VIII *Katna1/al1*$^{GCKO/GCKO}$ tubules
326 (Fig 4H). Moreover, analysis of cleaved caspase 3/7 immunolabelling revealed a 6.4 fold
327 increase in the number of apoptotic germ cells in *Katna1/al1*$^{GCKO/GCKO}$ versus
328 *Katna1/al1*$^{Flox/Flox}$ seminiferous tubules (Fig 4O). The majority of apoptotic cells were
329 spermatocytes that had stalled in anaphase I and meiosis II in stage I tubules (Fig 5J,N), and to
330 a lesser degree those undergoing metaphase I in stage XII (Fig 5J,N). In line with these defects,
331 analysis of epididymal sections confirmed almost no sperm reached the *Katna1/al1*$^{GCKO/GCKO}$
332 epididymis. The bulk of the cells in the lumen of *Katna1/al1*$^{GCKO/GCKO}$ epididymides were
333 instead prematurely sloughed round germ cells (Fig 4P, arrowheads).
334
335 Assessment of *Katna1/al1*$^{GCKO/GCKO}$ meiotic spindles, via the immunolabelling of testis
336 sections for α-tubulin, revealed that while meiotic spindles formed in *Katna1/al1*$^{GCKO/GCKO}$
337 spermatocytes, most were morphologically abnormal compared to *Katna1/al1*$^{Flox/Flox}$ controls

338 (Fig 5A,B). At metaphase, in contrast to the tightly packed morphology of *Katna1/al1*$^{Flox/Flox}$
339 controls (Fig 5Aa,Ba,e), chromosomes were loosely dispersed along the metaphase plate in
340 *Katna1/al1*$^{GCKO/GCKO}$ mice (4Bb,f). Misaligned and/or lagging chromosomes were frequently
341 observed in *Katna1/al1*$^{GCKO/GCKO}$ metaphase and anaphase spermatocytes (Fig 5A,B). As
342 detailed above, these defects ultimately lead to a large proportion of *Katna1/al1*$^{GCKO/GCKO}$
343 metaphase and anaphase spermatocytes stalling and undergoing apoptosis in stage XII-I
344 seminiferous tubules (Fig 4H, I-O). Of note, examination of *Katna1/al1*$^{GCKO/GCKO}$ stage I
345 tubules, revealed that these stalled metaphase and anaphase spermatocytes where characterised
346 by the ectopic accumulation of α-tubulin throughout their cytoplasm (Fig 5Ah,i) indicating
347 that KATNA1/KATNAL1-mediated severing restrains MT bulk in spermatocytes. Of the
348 subset of *Katna1/al1*$^{GCKO/GCKO}$ spermatocytes that progressed through meiosis, overtly normal
349 midbody formation was observed in telophase (Fig 5Ag,k). However, indicative of failure of
350 midbody to intracellular bridge conversion and similar to *Katna1*$^{GCKO/GCKO}$ mice, binucleated
351 spermatids were frequently observed in *Katna1/al1*$^{GCKO/GCKO}$ mice but never in
352 *Katna1/al1*$^{Flox/Flox}$ controls (Fig 5Ag,k). Consistent with compromised anaphase chromosome
353 segregation, abnormally large round spermatids were frequent in *Katna1/al1*$^{GCKO/GCKO}$ mice
354 but never in *Katna1/al1*$^{Flox/Flox}$ controls (Fig 5Ag,h). Collectively these data indicate that
355 KATNAL1 and KATNA1 can at least partially compensate for each other in metaphase and
356 anaphase of male meiosis. The frequency of binucleated spermatids in *Katna1/al1*$^{GCKO/GCKO}$
357 mice however, was similar to that of *Katnal1*$^{GCKO/GCKO}$ suggesting KATNA1 does not
358 compensate for KATNAL1 in cytokinesis.
359
360 Assessment of spermiogenesis in *Katna1/al1*$^{GCKO/GCKO}$ mice revealed that unlike the single
361 GCKO mice, acrosome biogenesis was overtly abnormal in the absence of both KATNA1 and
362 KATNAL1 indicating functional compensation between these two A-subunits (Fig 6A,B). In

363 PAS-stained *Katna1/al1*$^{Flox/Flox}$ control testis sections, a single PAS-positive acrosomal vesicle
364 was observed to adhere to step 2-3 round spermatid nuclei (stage II-III) in the Golgi phase of
365 acrosome development, and progressively spread to cover the apical half of the spermatid
366 nuclei as spermiogenesis progressed (Fig 6A). In *Katna1/al1*$^{GCKO/GCKO}$ mice however, a large
367 subset of round spermatids with supernumerary ectopic acrosomal vesicles were observed (Fig
368 6A orange arrowheads), in addition to a smaller subset of round spermatids wherein pro-
369 acrosomal vesicles had failed to attach to the nucleus at the appropriate time (Fig 6A, yellow
370 arrowheads). As spermiogenesis progressed, elongating spermatids with fragmented and
371 partially detached acrosomes were common in *Katna1/al1*$^{GCKO/GCKO}$, but never seen in
372 *Katna1/al1*$^{Flox/Flox}$ controls (Fig 6A, blue arrowheads). Ectopic PAS-positive vesicles were also
373 present throughout the seminiferous epithelium during multiple steps of acrosome biogenesis
374 in *Katna1/al1*$^{GCKO/GCKO}$, but not *Katna1/al1*$^{Flox/Flox}$, mice (Fig 6A, green arrowheads). TEM of
375 acrosome biogenesis confirmed these observations (Fig 6B), and revealed morphological
376 abnormalities in the spermatid Golgi apparatus of *Katna1/al1*$^{GCKO/GCKO}$ mice (Fig 6Bi,k)
377 compared to *Katna1/al1*$^{Flox/Flox}$ mice (Fig 6Bc,e). In normal round spermatids, and as seen in
378 *Katna1/al1*$^{Flox/Flox}$ mice (Fig 6Bc,e), the Golgi apparatus has a flattened sometimes horseshoe-
379 like morphology wherein the trans-Golgi network (TGN) is closely associated with, and
380 oriented in parallel to, the apical nuclear membrane. In *Katna1/al1*$^{GCKO/GCKO}$ mice however the
381 Golgi stacks were disorganised, often displaying a circular morphology, wherein the cis-Golgi
382 network almost entirely enclosed the TGN (Fig 6Bi), or a dispersed, splayed morphology (Fig
383 6Bk). These phenotypes, reveal KATNA1 and KATNAL1 collectively regulate the spatial
384 organisation of the Golgi apparatus and the transport of proacrosomal vesicles, and their fusion,
385 to the nuclear membrane. The acrosome abnormalities observed in *Katna1/al1*$^{GCKO/GCKO}$ mice,
386 are reminiscent of those seen in KATNB1 loss of function mice[11] suggesting these KATNA1
387 and KATNAL1 likely function in complexes with KATNB1 during acrosome biogenesis.

388

389 Analysis of the key MT-based structures required for spermiogenesis revealed phenotypes
390 consistent with a loss of MT severing and global dysregulation of the MT cytoskeleton. Similar
391 to *Katna1*$^{GCKO/GCKO}$ mice, immunolabelling of testis sections for acetylated tubulin revealed
392 sperm tails formed in *Katna1/al1*$^{GCKO/GCKO}$ mice, however reflective of sperm numbers fewer
393 tails were seen than in *Katna1/al1*$^{Flox/Flox}$ controls (Fig 6C-F). Acetylated tubulin staining
394 however, revealed the frequent ectopic accumulation of stable MTs in the cytoplasm of
395 spermatids in *Katna1/al1*$^{GCKO/GCKO}$ mice (Fig 6E-F), consistent with the decreased turnover of
396 MTs.

397

398 Assessment of manchette formation via the immunolabelling of testis sections for α-tubulin
399 revealed a catastrophic dysregulation of manchette formation. MTs accumulated around the
400 spermatid nucleus at stage VIII in *Katna1/al1*$^{GCKO/GCKO}$ mice (Fig 6G), however they failed to
401 assemble into a sheath around, and with MTs aligning in parallel to, the distal half of the
402 nucleus. Instead, the cytoplasm of the elongating spermatids became enriched in ectopic α-
403 tubulin as spermiogenesis progressed (Fig 6G). Analysis of elongating spermatid ultrastructure
404 via TEM confirmed these observations (Fig 6H). In *Katna1/al1*$^{Flox/Flox}$ mouse elongating
405 spermatids, a typical manchette structure wherein MTs projected distally from a perinuclear
406 ring was observed (Fig 6H). In *Katna1/al1*$^{GCKO/GCKO}$ mice, MTs were observed throughout the
407 cytoplasm of elongating spermatids, however these were never associated with a perinuclear
408 ring and were not arranged into typical manchette structure (Fig 6H). Collectively, these results
409 reveal that KATNA1/KATNAL1-mediated severing is required to restrain MT growth/prune
410 MT bulk during spermatid differentiation and to regulate manchette formation. Moreover, the
411 absence of these phenotypes in the single GCKO KATNA1 and KATNAL1 models, suggest
412 KATNA1 and KATNAL1 can compensate for each other in these aspects of spermiogenesis.

413

414 **KATNA1, KATNAL1 and KATNB1 interact with a range of cytoskeletal and vesicular**
415 **transport proteins in the mouse testis**

416 To explore the mechanism of action of KATNA1 and KATNAL1 during male meiosis and
417 spermiogenesis, and how they functionally compensate for each other, we determined the
418 respective interactome for KATNA1, KATNAL1 and KATNB1, within testis
419 immunoprecipitates via MS (Table S1 and Fig S6A-C). A total of 322, 108 and 213 proteins
420 were significantly enriched in the KATNA1, KATNAL1 and KATNB1 IP respectively
421 compared to their corresponding controls (Table S1 and Fig S6A-C). As expected, KATNA1,
422 KATNAL1 and KATNB1 were all significantly enriched in their own IPs validating the
423 specificity of each IP. KATNA1 and KATNAL1 were not found in the binding partner list for
424 each other, suggesting that they do not interact with each other to form heterohexamers (Table
425 S1). Similarly, neither bound to KATNAL2, however KATNAL1 and KATNB1 each pulled
426 the other down (Table S1). Consistent with the three proteins having similar functions, they
427 shared 48 candidate interacting proteins, in addition to 102 candidates that were shared by two
428 katanins (Fig S6D).

429

430 PANTHER protein class and gene ontology analysis[15] was conducted (Table S2 and
431 summarized in Fig S6E-J). Consistent with their regulation of MT-based processes in
432 spermatogenesis, KATNA1, KATNAL1 and KATNB1 each bound several cytoskeletal
433 proteins (Fig S6E-G, Table S2). Of particular relevance to the regulation of the Golgi and
434 acrosome formation all bound proteins involved in vesicle-mediated transport. In addition,
435 KATNA1 bound to known vesicle targeting proteins including ARL3 (Fig S6E-G, Table S2).
436 Functional descriptions of selected cytoskeletal, membrane/vesicle-transport and

437 spermatogenesis related proteins significantly enriched in the KATNA1, KATNAL1 and
438 KATNB1 IP experiments are summarised in Table S3.
439
440 Strikingly, across the three IP experiments the cytoskeletal proteins identified were
441 predominantly actin-related proteins, however tubulin and MT-related proteins were also
442 identified (Fig S6E-J, Table S2 and S3). KATNA1 also bound to the intermediate filament
443 protein vimentin (Table S2 and S3). Of the MT-related proteins identified as katanin testis-
444 interactors, multiple proteins involved in the regulation and activity of dynein MT motor
445 proteins were identified. Indeed, KATNA1 and KATNB1 both bound components of the
446 dynactin complex (Table 1), an essential cytoplasmic-dynein cofactor involved in MT-based
447 cargo transport. KATNA1 also bound DNAAF4, which is required for axonemal dynein
448 assembly and thus ciliary motility, and all three katanins bound NUDC, a dynein-dynactin
449 complex regulator (Table S3). Consistent with the phenotypes of our *Katnb1*[11,12], *Katnal1* and
450 *Katna1/al1* mutant mice, the MT-related proteins identified included those with established
451 functions in the mitotic and/or meiotic spindle (e.g. NUDC, MAPRE1/EB1), intraflagellar
452 transport and ciliogenesis (ARL3) and axoneme assembly DNAAF4; Table S3). Moreover,
453 several have previously been implicated in spermatogenesis and male fertility (e.g. ARL3,
454 DNAAF4, MAPRE1/EB1) and, consistent with its mechanism of action, KATNA1 pulled
455 down both α- and β-tubulin isoforms (Table S3).
456
457 Of the actin-binding proteins identified across the three katanin IP experiments, multiple
458 regulators of actin polymerization/dynamics were identified including components of the
459 ARP2/3 and CapZ complexes (Table S2, S3). KATNA1, KATNAL1 and KATNB1 each bound
460 at least two components of the ARP2/3 complex. Data strongly suggests this complex plays
461 key roles in blood-testis-barrier integrity, spermiogenesis and spermiation[16-19]. Likewise, all

462 bound the CapZ subunit CAPZA1, and KATNA1 and KATNAL1 both bound CAPZA2. In
463 addition, several regulators of actin-network organization were identified to bind KATNA1
464 and KATNB1, and KATNA1 bound MYL6, an actin motor protein which localizes to the
465 manchette (Table S3). Collectively, these data indicate a novel connection between katanin
466 proteins and the actin cytoskeleton in male germ cells. This is consistent with data showing the
467 *Arabidopsis* katanin A-subunit KATANIN1 regulates the actin cytoskeleton[20] and that cortical
468 localisation of *Drosophila* KATNA1 orthologue kat-60 is actin-dependent[21].
469
470 KATNA1 and KATNB1 bound multiple Rab GTPases, a family which regulates multiple
471 aspects of vesicle transport (vesicle budding, actin/MT-mediated transport and fusion) (Tables
472 1, S1 and S2). Of note in spermatogenesis there is increasing evidence Rab and Rab-like
473 proteins mediate pro-acrosomal vesicle transport, in addition to intraflagellar transport and
474 sperm tail development[22-25]. Other transport proteins included those related to endoplasmic
475 reticulum (ER) to Cis-Golgi transport, intra-Golgi transport, clathrin-mediated vesicle
476 disassembly and endocytosis (Table 1). Further consistent with the acrosome defects in
477 *Katna1/al1*$^{GCKO/GCKO}$ mice, KATNAL1 bound ACRBP a protein essential for acrosome granule
478 formation and maintenance of acrosome integrity, and consistent the Golgi defects, a number
479 of proteins were identified with roles in Golgi organization (e.g. Rab2, Rab6, VCP, LMAN1;
480 Table S3).
481
482 Other notable proteins identified as binding the katanins included essential male meiosis
483 regulators TEX15 (KATNA1 IP) and HSPA2 (KATNA1/B1 IP), and FABP9 a protein required
484 for normal sperm head shape in mice (KATNA1/AL1 IP) (Table S3).
485
486 **Discussion**

487 Katanin MT severing enzymes are potent regulators of MT dynamics and organization across
488 eukaryotes. Herein, using a combination of single and double katanin A-subunit GCKO mice,
489 we show for the first time the essential requirement for katanin A-subunits in mammalian male
490 meiosis, provide the first direct evidence that different katanin A-subunits can functionally
491 compensate for one another and establish KATNA1 and KATNAL1 as novel regulators of
492 spermatid differentiation (spermiogenesis). Specifically, KATNA1 and KATNAL1
493 collectively regulate spermatocyte metaphase and anaphase spindle structure and function,
494 acrosome development via the Golgi apparatus and pro-acrosomal vesicle trafficking, sperm
495 head shaping via manchette formation, and collectively restrain MT bulk during male meiosis
496 and spermiogenesis. In addition to this, KATNAL1 regulates spermatocyte cytokinesis, sperm
497 tail and HTCA development, manchette dynamics and dissolution, and the release of sperm
498 from the seminiferous epithelium (spermiation). Through the analysis of KATNA1,
499 KATNAL1, and KATNB1 testis binding proteins, we reveal these activities involve
500 interactions with a diverse suite of proteins, including actin-, MT-, vesicle/membrane
501 trafficking-, and spermatogenesis-related proteins.
502
503 The finding that KATNA1 and KATNAL1, but not KATNA1 and KATNAL2, have gene
504 redundancy in mammalian spermatogenesis is consistent with the highly similar domain
505 structure and severing activity shared between KATNA1 and KATNAL1, but not KATNAL2
506 [2]. Interestingly, KATNAL1 fully compensates for KATNA1 germ cell loss, whereas KATNA1
507 can only partially compensate for germ cell KATNAL1 loss. This suggests KATNAL1 is the
508 more potent/efficient MT severing enzyme in the testis, and/or that it has neofunctionalized to
509 acquire additional functions. We predict it is a combination of the two. Indeed, KATNAL1 has
510 possesses higher MT severing activity in mouse Neuro-2a cells, and is less prone to degradation
511 in HEK293T cells compared to KATNA1[26]. However, we also identified several different

512 KATNA1 versus KATNAL1 testis interacting proteins indicating they have at least some
513 distinct modes of regulation and/or function. These findings have important implications for
514 the study of katanin proteins in contexts wherein multiple A-subunits exist, revealing that
515 discovery of full katanin function can require double KO models.
516
517 We identify KATNA1/KATNAL1 as essential regulators of metaphase and anaphase spindle
518 structure, metaphase chromosome alignment, anaphase chromosome segregation and,
519 KATNAL1 as a cytokinesis regulator during male meiosis. While a role for katanin A-subunits
520 in male mammalian meiosis has never previously been shown, we have previously shown the
521 B-subunit, KATNB1 is essential for normal spindle architecture and function, and for
522 cytokinesis in mouse spermatocytes[11,12]. In strong support of these overlapping functions being
523 due to KATNB1 working in partnership with KATNA1 and KATNAL1, KATNB1-KATNA1
524 and KATNB1-KATNAL1 complexes are present throughout mouse male meiosis wherein they
525 localize to spindle MTs[11]. That single GCKO of KATNAL1, but not KATNA1, is sufficient to
526 cause meiotic defects, agrees with our previous data showing KATNB1-KATNAL1 complexes
527 are the most abundant type of katanin complex during male meiosis[11].
528
529 The misalignment of metaphase chromosomes, followed by uneven anaphase segregation in
530 *Katnal1*$^{GCKO/GCKO}$ and *Katna1/al1*$^{GCKO/GCKO}$ meiosis is consistent with KATNA1/KATNAL1
531 regulating MT-chromosome attachment and/or regulating spindle dynamics via metaphase
532 poleward 'flux' (reviewed in[27]) and anaphase 'Pacman-flux' (reviewed in[28]). While future
533 studies will need to directly test this in meiosis, katanin-mediated MT severing has been shown
534 to directly contribute to metaphase spindle flux in HEK293 mitotic cells[29] and Pacman-flux in
535 *Drosophila* mitotic cells[30].

536

537 The role for KATNAL1 in cytokinesis identified herein aligns with evidence that midbody
538 disassembly in mitosis requires MT severing ([31] and reviewed in [2]) and our own data, regarding
539 KATNB1 function in mouse male meiosis[11,12]. That only a subset of germ cells fails cytokinesis
540 in the absence of KATNAL1 or KATNB1, suggests that other MT severing enzymes must also
541 be involved in this process. Indeed, we have recently shown the related MT severing enzyme,
542 spastin, also contributes to cytokinesis during male meiosis[32].

543

544 Our data establishes KATNA1 and KATNAL1 as novel regulators of Golgi organisation and
545 pro-acrosomal vesicle trafficking and fusion during acrosome biogenesis. This contributes to
546 an emerging body of evidence that MT-severing enzymes regulate vesicle-based transport in
547 spermiogenesis, as we have recently shown spastin and KATNB1 are also essential for pro-
548 acrosomal vesicle transport and fusion events[11,32]. The contribution of KATNA1/KATNAL1 to
549 these processes may be as simples as a role in pruning the MT tracks along which Golgi
550 membranes are spatially positioned and pro-acrosomal vesicles are delivered. However, the
551 interaction of KATNA1, KATNAL1 and KATNB1 with multiple proteins involved in Golgi
552 organisation and vesicle trafficking suggests a more direct role and raises the possibility MT-
553 severing can modulate cargo-MT interactions.

554

555 We have previously shown KATNAL2 is essential for sperm tail development via basal body
556 -plasma membrane docking and the initiation of spermatid axoneme extension[5]. Here, we show
557 KATNAL1 is also required, but in the subsequent assembly, and potential stability, of axoneme
558 MT doublets, and in mitochondrial sheath and ODF development. Moreover, while KATNAL1

559 is not required for basal body-membrane docking, it is required for HTCA formation/integrity.
560 The precise mechanism of KATNAL1 contribution to these processes remains an outstanding
561 question. One possibility is that KATNAL1-mediated MT severing directly amplifies and
562 regulates MTs for axoneme doublet formation and HTCA fortification. However, the
563 variability in phenotypes (e.g. missing MT doublets in some tails and supernumerary MT
564 doublets in others), is more suggestive of mis-regulated cargo trafficking. Of note, and
565 consistent with the co-incident manchette defects in KATNAL1 loss, sperm tail components
566 including the ODFs, and proteins required to strengthen the HTCA appear to be delivered via
567 the MTs of the manchette, and abnormal sperm tail and manchette phenotypes often occur in
568 parallel (reviewed in[33]). It is thus possible that the abnormal manchette phenotypes in
569 *Katnal1*$^{GCKO/GCKO}$ mice underpin at least some of the sperm tail defects.

570

571 The manchette phenotypes identified in the *Katnal1*$^{GCKO/GCKO}$ mice establish roles for
572 KATNAL1 in manchette migration down the sperm nucleus, which requires 'unzipping' of
573 rod-like manchette-nuclear linkers, and in controlling manchette MT length and in manchette
574 MT disassembly. These functions are consistent with a direct MT-severing mechanism.
575 Strikingly, the *Katnal1*$^{GCKO/GCKO}$ mouse manchette phenotypes, mirror not only those in
576 KATNB1 loss of function mice[11,12], but also those in KATNAL2 loss[5]. These identical yet non-
577 redundant KATNAL1 and KATNAL2 phenotypes suggest the two proteins are executing
578 similar functions in the manchette but severing different MT subpopulations. This is consistent
579 with our proteomics data, demonstrating KATNAL2 is not a binding partner of KATNAL1.

580

581 Similar to the established roles of Sertoli cell KATNAL1 is required to maintain round
582 spermatid-Sertoli cell adhesion[13]. We show germ cell KATNAL1 is involved in spermatid
583 retention and elongated spermatid release via spermiation. Data is consistent with KATNAL1
584 severing the cytoskeletal connections tethering elongating spermatids to the Sertoli cell. The
585 precise cytoskeletal targets of this action need to be identified, but of note, our IP revealed
586 katanins interact with multiple ARP2/3 complex proteins. The ARP2/3 complex appears to
587 facilitate spermiation, *albeit* via the disassembly of the Sertoli cell actin cytoskeleton [19]. Of
588 note spermiation defects in KATNAL2 mutant mice [5], and spermatid adhesion and spermiation
589 defects seen in the KATNB1 mutant mice[11,12] phenocopy those seen in *Katnal1*$^{GCKO/GCKO}$ mice.
590 This suggests that KATNAL1-KATNB1 complexes along with KATNAL2-KATNB1
591 complexes facilitate spermatid release.

592

593 Finally, we defined the testis interactome for KATNA1, KATNAL1 and KATNB1. While a
594 katanin interactome has previously been defined in HELA cells[4], this is the first *in vivo* tissue
595 wide interactome for each protein. A number of protein classes were identified that we predict
596 are related to the activation/inhibition of katanin function (e.g. metabolite interconversion
597 enzymes). Of proteins that we predict are involved specific testis functions of the katanin
598 enzymes, cytoskeletal and vesicle-transport related proteins emerged as key protein classes.
599 Future studies will need to define precise nature of these interactions, however they paint a
600 picture of katanin action involving a complex crosstalk between different cytoskeletal networks
601 notably between actin and MT networks, and suggest a direct role for katanins in regulating
602 the interaction of dynein- and vesicle-based cargo machinery with MTs.

603

604 Collectively, this study establishes KATNA1 and KATNAL1 as novel players in male germ
605 cell MT regulation. The data defined herein, taken together with our previous data on the roles
606 of KATNB1[11,12], KATNAL2[5] and Sertoli cell KATNAL1[13], allows us to define a model of the
607 complete katanin 'toolbox' during mammalian spermatogenesis (Fig 7). This data
608 unequivocally shows the emergence of multiple katanin A-subunits in higher eukaryotes, not
609 only allows for functional sub-specialization and thus customized cutting of discrete MT
610 subpopulations, but also for the protection of katanin function in critical processes such as
611 meiosis through gene redundancy.

612

613

614 **Methods**

615

616 **Mouse model production**

617 All animal procedures were approved by the Monash University School of Biological Sciences
618 Animal Experimentation Ethics Committee and the University of Melbourne Ethics committee
619 and conducted in accordance with National Health and Medical Research Council (NHMRC)
620 Guidelines on Ethics in Animal Experimentation.

621

622 To the generate *Katna1*$^{Flox/Flox}$ mice, *Katna1* KO-first conditional-ready mice (*Katna1*$^{KO/WT}$)
623 were generated through the Monash University Node of the Australian Phenomics Network
624 using a EUCOMM *Katna1* KO-first conditional-ready ES clone (EPD0586_1_B10) as
625 described[34]. To disrupt the *Katna1* gene, the FRT-LacZ-loxP-Neo-FRT-loxP-*Katna1-exons6-*
626 *7*-loxP cassette was inserted into intron 5 of the *Katna1* gene (Fig S1C). To generate
627 conditional *Katna1* mouse (*Katna1*$^{Flox/Flox}$), mice heterozygous for the knockout-first allele
628 (*Katna1*$^{KO/WT}$) were then crossed with a transgenic line carrying the *Flp* recombinase gene.

629 This resulted in removal of the *FRT* flanked gene-trap cassette, exposing a floxed *Katnal1* exon
630 6-7 and reverting mice to a wild-type phenotype. *Katna1*$^{GCKO/GCKO}$ were then generated using
631 a two-step breeding strategy. (1) *Katna1*$^{Flox/Flox}$ females were mated with a *Stra-8-cre*
632 transgenic line to produce *Katna1*$^{WT/Flox,Stra8\text{-}cre+}$ males. (2) *Katna1*$^{WT/Flox,Stra8\text{-}cre+}$ males were
633 mated with *Katna1*$^{Flox/Flox}$ females to produce *Katna1*$^{Flox/Flox,Stra8\text{-}cre+}$ progeny
634 (*Katna1*$^{GCKO/GCKO}$). In these mice, gene disruption relied on Cre-lox recombination mediated
635 excision of *Katna1* exons 6 and 7 (ENSMUSE00001254109, ENSMUSE00001247569), and
636 the *Stra8-Cre* used is expressed from late spermatogonia onwards [35].
637
638 *Katnal1*$^{Flox/Flox}$ mice, wherein exon 3 (ENSMUSE00001360953) of the *Katnal1* gene is flanked
639 by loxP sites, were generated by the Monash Genome Modification Platform using
640 CRISPR/Cas9 technology. Guide RNA target sites flanking the target exon (5' end of exon -
641 5' TCAATGTCTGAGGTGGATAA 3' and 3' end of exon - 5'
642 CAAAGAAGTCTTTTAGACCC 3') were identified using the UCSC Genome Browser. A
643 single stranded DNA homology directed repair template, was generated from a *Katnal1*
644 conditional KO targeting construct using the Guide-it Long ssDNA Strandase Kit (Takara,
645 632645). The following oligonucleotides were used to generate a PCR product from which the
646 ssDNA was generated: 5'/5Biosg/GATGCTTAGCACTGGCTGG 3' and 5'
647 GAACGTGTGCTATTTGGTCTTTAAG 3'. The CRISPR/Cas9 ribonucleoprotein complex
648 and single stranded DNA homology repair templates were microinjected into C57BL/6J
649 zygotes at the pronuclei stage and transferred into the uterus of pseudo-pregnant females.
650 *Katnal1*$^{GCKO/GCKO}$ mice were generated by intercrossing *Katnal1*$^{Flox/Flox}$ mice with a *Stra8-cre*
651 transgenic line as above. *Katnal2*$^{Flox/Flox}$ mice were generated as previously described[5].
652 *Katna1/al1*$^{Flox/Flox}$ and *Katna1/al2*$^{Flox/Flox}$ mice were generated by breeding *Katna1*$^{Flox/Flox}$ mice
653 with either *Katnal1*$^{Flox/Flox}$ or *Katnal2*$^{Flox/Flox}$ mice, respectively. Double germ cell deletion was

654 then achieved using by intercrossing double floxed mice with a *Stra8-cre* transgenic line as
655 above.
656
657 All mice were maintained on a C57BL/6 background. To control for background strain effects
658 on phenotype, *Katna1*$^{Flox/Flox}$, *Katnal1*$^{Flox/Flox}$, *Katna1/al1*$^{Flox/Flox}$ and *Katna1/al2*$^{Flox/Flox}$ mice
659 mice were used as controls for *Katna1*$^{GCKO/GCKO}$, *Katnal1*$^{GCKO/GCKO}$, *Katna1/al1*$^{GCKO/GCKO}$ and
660 *Katna1/al2*$^{GCKO/GCKO}$ mice, respectively. Mouse genotypes were determined from tail biopsies
661 using real time PCR with specific probes designed for each allele (Transnetyx, Cordova, TN).
662 Efficiency of exon excision in *Katna1*$^{GCKO/GCKO}$, *Katnal1*$^{GCKO/GCKO}$, *Katna1/al1*$^{GCKO/GCKO}$ and
663 *Katna1/al2*$^{GCKO/GCKO}$ mice, was determined by qPCR of isolated germ cells as described below.
664 Protein levels were determined by western blotting of germ cell and testis lysates as described
665 below.
666
667 **Quantitative qPCR**
668 Purified germ cells were prepared via the STAPUT method as detailed in [36]. Total RNA was
669 then extracted from purified germ cells using Trizol (Life Technologies), and reverse-
670 transcribed into cDNA using SuperScript III Reverse Transcriptase (Life Technologies).
671 Primers spanning *Katna1* exons 6 and 7 (5'-TCAGGAAGCAGTGGTGTTACC-3' forward
672 and 5'-AAGGGTCTTTCCAGTGCCAG-3' reverse), *Katnal1* exons 3 and 4 5'-
673 CCGTGTCTTGCCGAGATGAA-3'forward and 5'-GCGATTTGGACGCCTGATTT-3'
674 reverse) and *Katnal2* exons 2 and 3 (5'-AAGGCTTTGGAGGAGGAGAC-3' forward and 5'-
675 GGGGCCTTCTTAACCACTTT-3') were used to verify gene deletion in the corresponding
676 mouse models. All qPCRs were performed using SYBR Select Master Mix (Applied
677 Biosystems). Each reaction was performed in triplicate using the Agilent Mx3000P qPCR
678 system or an Applied Biosystems QuantStudio 3 Real-Time PCR System with the parameters

679 of 50°C for 2 minutes, 95°C for 10 minutes followed by 40 cycles of 95°C for 15 seconds and
680 60°C for 1 minute. *Ppia* was amplified at the same time as an internal control (using 5'-
681 CGTCTCCTTCGAGCTGTTT-'3 forward and 5'-CCCTGGCACATGAATCCT-'3 reverse
682 primers), and all results were normalized to *Ppia* expression. Differential expression was
683 analysed using the $2\Delta\Delta^{CT}$ method[37].
684
685 **Male fertility characterisation**
686 Male fertility of all mouse models was characterised as per[38]. Male fertility was assessed by
687 mating 10-12 week old males with wild-type females (≥6 weeks of age). Copulatory plugs
688 were monitored to confirm successful mating and the number of pups born per copulatory plug
689 was recorded. Each male was test mated with 2-3 females and pup numbers averaged. Testis
690 daily sperm production (DSP) and total epidydimal sperm content were determined using the
691 Triton X-100 solubilisation method[39] (n≥3/genotype) as modified in[11]. To assess sperm
692 motility, sperm were backflushed as per[40] from cauda epididymides and motility was assessed
693 using a computer assisted sperm analyser, as described previously[41].
694
695 For histology, testis and epididymal tissue were fixed in Bouin's fixative and histology
696 assessed using standard methods. Male reproductive tract histology was visualised using
697 periodic acid-Schiff's (PAS) and haematoxylin staining, and air-dried caudal epididymal sperm
698 smears were visualised using haematoxylin and eosin staining (n≥3/genotype). Germ cell
699 apoptosis was evaluated by immunostaining for cleaved Caspase 3 and 7 as per[42] and as
700 described below. The number of Caspase-positive cells in a minimum of 50 randomly selected
701 seminiferous tubules per mouse were counted and statistical analysis conducted as described
702 below and as per[11](n≥3 mice /genotype).
703

704 **TEM**

705 For analysis of seminiferous tubule ultrastructure, partially decapsulated testes and cauda
706 epididymides were fixed with 5% glutaraldehyde/4% paraformaldehyde/0.02% picric acid in
707 0.1 M sodium cacodylate buffer, pH 7.4. as per[11]. Samples were *en bloc* stained with 2% uranyl
708 acetate and all samples were embedded into Epon resin using standard procedures. Ultrathin
709 sections were cut on a Leica EM UC7 Ultramicrotome and placed on Copper 100×100 square
710 grids (ProSciTech). Sections were analysed using a FEI Talos L120CI TEM in the Ian Holmes
711 Imaging Centre (The University of Melbourne, Parkville)

712

713 **Antibody use**

714 Primary antibodies used included those against acetylated-tubulin (T6793, Sigma, RRID:
715 Ab_477585, ascites fluid, 1 in 10,000), α-tubulin (T5168, Sigma, ascites fluid, 1 in 50,000),
716 cleaved-Caspase 3 (9664, Cell Signalling, 0.5 μg ml^{-1}), cleaved-Caspase 7 (9491, Cell
717 Signalling, 0.23 μg ml^{-1}), KATNA1 (as described previously [11]), KATNAL1 (as described
718 previously[11]), KATNB1 (as described in [11]), SUN5 (ProteinTech 17495-1-AP 0.8 μg/ml) and
719 TUBB3 (Sigma-Aldrich, SAB3300047, 0.15 μg ml^{-1}). Secondary antibodies included Alexa
720 Fluor 488 donkey anti-mouse (A212062 Invitrogen), Alexa Fluor 488 donkey anti-rabbit
721 (A21206, Invitrogen), and Alex Fluor 555 donkey anti-rabbit (A31572, Invitrogen). EnVision+
722 Dual Link System-HRP (K4063, Dako) was used to amplify signal. The specificity of
723 immunolabelling was determined by staining sections in parallel in the absence of primary
724 antibody or where available KO mouse tissue.

725

726 **Western blotting**

727 Proteins were extracted from STAPUT purified germ cells [36], and immunoblotting conducted
728 as previously described[36]. Images were captured using a ChemiDoc MP Imaging System

729 (BioRad). The molecular weights of detected proteins were estimated using a PageRuler Plus
730 Prestained Protein Ladder (ThermoFisher) and the Image Lab 6.0 Molecular Weight Analysis
731 Tool (BioRad).
732
733 **Immunochemistry and imaging**
734 To assess KATNA1 testis localisation, 5 μm cryostat testis sections were fixed in 1:1 methanol-
735 acetone and permeabilised in 0.2% Triton X-100 in PBS as per[43]. To assess testis localisation
736 of all other proteins, Bouin's fixed testes were processed into paraffin and 5 μm sections
737 prepared using standard methods. Paraffin sections were dewaxed and heat-mediated antigen
738 retrieval was conducted by microwaving sections 10 mM citrate buffer (pH 6) for 16 minutes
739 as per [44]. For sections to be used for chromogenic immunohistochemistry (α-tubulin,
740 acetylated-tubulin, cleaved-caspase 3 and 7), endogenous peroxidase activity was then blocked
741 via incubation with 5% H_2O_2 for 5 minutes. For all testis immunolabelling, non-specific protein
742 binding was minimised by incubation with CAS-block (Invitrogen) for 30 minutes and sections
743 were then incubated with primary antibodies diluted in DAKO Antibody Diluent overnight at
744 4°C. For immunofluorescent labelling, sections were incubated with the appropriate Alexa
745 Fluor secondary antibodies diluted 1in 500 for 1 hour at room temperature. DNA was then
746 visualised using 1 μg ml^{-1} 4',6-diamidino-2-phenylindole (DAPI, Invitrogen) or 4 μM TO-
747 PRO-3 Iodide (TOPRO, Thermo Scientific). Acrosomes were visualized using 0.5 μg ml^{-1}
748 lectin peanut agglutinin (PNA), Alexa Fluor 488 conjugate (L21409, Life Technologies). For
749 chromogenic immunohistochemistry, sections were incubated with DAKO EnVision+ Dual
750 Link System-HRP for 30 minutes at room temperature. The Liquid DAB+ Substrate
751 Chromogen System (DAKO, K3468) was then applied as per the manufacturer's instructions.
752 Nuclei were counterstained using Mayer's haematoxylin (Amber Scientific), followed by
753 Scott's tap water (Amber Scientific).

754

755 To assess SUN5 localisation in cauda epididymal sperm, sperm were washed in PBS and
756 airdried onto slides. Sperm were then fixed in 4% paraformaldehyde for 10 minutes. Sperm
757 were then permeabilised, blocked for non-specific protein binding and immunofluorescently
758 labelled as above.

759

760 Immunofluorescent images were collected using a Leica TCS SP8 confocal microscope (Leica
761 Microsystems) at the Monash Micro Imaging (Monash University) and the University of
762 Melbourne Biological Optical Microscopy Unit (University of Melbourne, Parkville). A
763 63x/1.40 HC PL APO CS2 oil immersion objective was used to take all immunofluorescent
764 images. Bright field images were collected cellSens Imaging Software (Olympus) on an
765 Olympus BX53 light microscope equipped with an Olympus DP80 camera.

766

767 **IP-MS**

768 For IP assays, wild-type mouse testes (n=3 per IP assay) were lysed in 1% NP-40 (PBS)
769 supplemented with protease inhibitor cocktail (Calbiochem, 539134). KATNA1, KATNAL1
770 and KATNB1 and their binding partners were then co-immunoprecipitated using the Pierce
771 Co-immunoprecipitation Kit (Thermo Scientific, 26149) as per the manufacturer's instructions,
772 in combination with either our KATNA1 (10µg per IP column), KATNAL1 (5µg) or KATNB1
773 (5µg) inhouse antibody. Briefly, to reduce non-specific binding, testis protein lysates were first
774 pre-cleared by incubation with 400µl of Pierce control agarose resin slurry for a 0.5-1 hour at
775 4°C with gently rocking. For each pre-cleared testis lysate, 5 mg was then loaded into two IP
776 columns, one which contained the target antibody covalently coupled to the amine reactive
777 Pierce AminoLink Plus Coupling Resin and one which contained the target antibody and a
778 non-amine reactive Pierce Control Agarose Resin (negative control), and incubated overnight

779 at 4°C. Lysate flow through was removed, columns were washed and bound protein eluted and
780 collected as per the manufacturer's instructions. The eluted proteins were neutralised with
781 1.5M Tris-HCL (pH 8.8), reduced with TCEP, then digested by incubation with trypsin
782 overnight at 37°C. Peptide samples were freeze dried and resuspended in 2% acetonitrile
783 (ACN)/0.1% formic acid (FA) (diluted in MilliQ water) before concentrated FA was added to
784 adjust the pH to <3. Samples were purified using reverse-phase chromatography C18 stage
785 tips, which aim to desalt and fractionate in-solution peptides at an acidic pH. The tips were
786 initially activated with 100% methanol and equilibrated with 0.1% FA, before samples were
787 loaded into them and desalted with 0.1% FA. Peptides were eluted with 80% ACN/0.1% FA,
788 freeze dried, resuspended in 2% ACN/0.1% FA and sonicated for 15 minutes in a water bath.

789 The purified peptide samples were analysed via nano liquid chromatography coupled to tandem
790 mass spectrometry (LC-MS/MS). Briefly, the KATNA1 IP and KATNB1 IP samples were
791 analysed at the Monash Proteomics and Metabolomics Facility (Monash University) using an
792 Orbitrap Fusion Tribrid mass spectrometer (ThermoFisher, USA) and a Q-Exactive Hybrid
793 Quadrupole - Orbitrap mass spectrometer (ThermoFisher, USA), respectively. Both
794 instruments were coupled to an UltiMate 3000 RSLCnano system (ThermoFisher, USA)
795 equipped with an Acclaim PepMap RSLC C18 nanoViper Analytical Column (100Å, 75 µm
796 X 50 cm, 2 µm; ThermoFisher, USA) and an Acclaim PepMap 100 C18 HPLC nanoViper Trap
797 Column (100Å, 100 µm X 2 cm, 5 µm; ThermoFisher, USA). The tryptic peptides were
798 separated by increasing concentrations of 80% acetonitrile (ACN) / 0.1% formic acid at a flow
799 rate of 250 nl/min for 128 min and 158 min, respectively. Both mass spectrometers were
800 operated in data-dependent acquisition (DDA) mode to automatically switch between full scan
801 MS and MS/MS acquisition. Each survey full scan (m/z 375–1800) in the Orbitrap Fusion
802 Tribrid acquisitions was acquired in the Orbitrap with 120,000 resolution (at m/z 200) after
803 accumulating ions to a Normalised AGC Target of 250% with a maximum injection time of 54

804 ms. Dynamic exclusion was set to 15 seconds. Adhering to a 2 sec cycle time, the most intense
805 multiply charged ions ($z \geq 2$) were sequentially isolated and fragmented in the collision cell by
806 higher-energy collisional dissociation (HCD) and ms2 scans were acquired with a fixed
807 injection time of 54 ms, 30,000 resolution and a Normalised AGC Target of 400%. Very similar
808 parameters were used for the Q-Exactive Hybrid Quadrupole – Orbitrap acquisitions.

809 The KATNAL1 IP purified peptide samples were analysed at the University of Melbourne
810 Mass Spectrometry and Proteomics Facility, using an Orbitrap Eclipse Tribrid Mass
811 Spectrometer (ThermoFisher, USA) equipped with a nano ESI interface coupled to an Ultimate
812 3000 nano HPLC (Thermo Fisher, USA). The LC system was equipped with an Acclaim
813 Pepmap 100 C18 HPLC nanoViper Trap Column (100 Å, 75 µm X 2 cm, 3 µm; ThermoFisher,
814 USA) and an analytical column as above. The enrichment column was injected with the tryptic
815 peptides (1 µL, 100 ng) at an isocratic flow of 5 µL/min of 2% *v/v* CH_3CN containing 0.05%
816 *v/v* trifluoroacetic acid for 6 min, applied before the enrichment column was switched in-line
817 with the analytical column. The eluents were 0.1% v/v formic acid (solvent A) in H_2O and
818 100% *v/v* CH_3CN in 0.1% *v/v* formic acid (solvent B). The gradient was at 300 nl min^{-1} from
819 (i) 0–6 min, 3 % B; (ii) 6–35 min, 3–23 % B; (iii) 35-45 min, 23-40 % B; (iv) 45-50 min, 40-
820 80 % B; (v) 50-55 min, 80–80 % B; (vi) 55-55.1 min, 80-3 % B; (vii) 55.1-65 min, 3-3 % B.
821 The Eclipse Orbitrap mass spectrometer was operated in the data-dependent mode, wherein
822 full MS^1 spectra were acquired in a positive mode over the range of *m/z* 375-1500, with spray
823 voltage at 1.9kV, source temperature at 275 °C, MS^1 at 120,000 resolution, normalized AGC
824 target of 100 % and maximum IT time of 22 ms. The top 3 second method was used and
825 selecting peptide ions with charge states of ≥ 2-7 and intensity thresholds of ≥ 5E4 were
826 isolated for MS/MS. The isolation window was set at 1.6 *m/z*, and precursors were fragmented
827 using higher energy C-trap dissociation (HCD) at a normalised collision energy of 30, a
828 resolution of 15,000, a normalized AGC target of 100% and automated IT time.

829

830 The raw MS data were analysed with the MaxQuant software suite for the identification and
831 quantification of peptides/proteins from the Mouse SwissProt database. Fixed modifications of
832 carbamidomethylation of cysteine as well as variable oxidation of methionine and protein N-
833 terminal acetylation were considered. Trypsin/P was set as the protease with a maximum of 2
834 missed cleavages. Statistical analysis was conducted with the Perseus software considering
835 protein and PSM false discovery rates (FDR) both set at < 0.01. For each IP assay, the majority
836 UniProt ID(s) for each significantly enriched protein group were then analysed using
837 PANTHER Gene Ontology and protein classification[15].

838 **Statistics**

839 Statistical analysis of germ cell apoptosis data was conducted in R version 3.5.1[45]. Generalised
840 linear mixed (GLM) models were used to compare the number of caspase-positive cells per
841 tubule across genotypes, with animal ID included as a random effect to account for repeated
842 measures per individual. For each model, Akaike information criteria (AIC) estimates were
843 used to select the most appropriate error distribution and link function (i.e. poisson, negative
844 binomial, zero-inflated poisson, zero-inflated negative binomial) using the glmer function
845 (lme4 package[46]) and glmmTMB function (glmmTMB, package[47]). For all models, a zero-
846 inflated negative binomial distribution (fitted with glmmTMB, using the ziformula argument)
847 was selected as the most appropriate error distribution and link function (i.e. had the lowest
848 AIC score).

849

850 All other statistical analysis, other than for the proteomics (described above), was conducted
851 in Graphpad Prism 9.0. The statistical significance of differences between two groups was
852 determined with an unpaired Student t-test. Significance was defined as a P value of <0.05.

Acknowledgements

We thank Dr Liza O'Donnell and Dr Duangporn Jamsai for advice on the initial stages of the project. We thank Ms G. Gemma Stathatos, Ms Lauren Rogers and Ms Georgia Shering for technical assistance. We thank Associate Professor Nicholas Williamson, Dr Ching-Seng Ang and Dr Michael Leeming for technical assistance and advice regarding the MS analysis. We thank the following platforms for the use of their facilities and services: at The University of Melbourne (Parkville), the Biological Optical Imaging Platform, the Ian Holmes Imaging Centre, the Mass Spectrometry and Proteomics Facility, the Melbourne Bioresources Platform and the Melbourne Histology Platform; and at Monash University (Clayton), the Monash Animal Research Platform, the Monash Gene Modification Platform, the Monash Histology Platform, Monash Micro Imaging and the Monash Proteomic and Metabolomic Facility.

Author Contributions

Conceptualisation, J.E.M.D, M.K.O; Methodology, J.E.M.D, A.E.O, D.J.M, R.B.S, B.J.H and M.K.O; Formal Analysis, J.E.M.D, M.G, K.W, A.E.O, D.J.M, J.N, R.B.S, B.J.H, M.K.O; Investigation, J.E.M.D, M.G, K.W, A.E.O, D.J.M, J.N, R.B.S, B.J.H; Writing – Original Draft, J.E.M.D, M.G, M.K.O; Writing – Review & Editing, J.E.M.D, R.B.S, M.K.O; Visualisation, J.E.M.D, M.G, K.W; Supervision, J.E.M.D, M.K.O; Project Administration, J.E.M.D, M.K.O; Funding Acquisition, M.K.O

Declaration of interests

The authors declare no competing or financial interests.

Funding

878 J.E.M.D is supported by a National Health and Medical Research Council Ideas Grant to
879 M.K.O and J.E.M.D (APP1180929) and this project was supported in part by funding from the
880 National Health and Medical Research Council of Australia (APP1138014) and the Australian
881 Research Council (DP160100647). B.J.H is supported by funding from the Male Contraceptive
882 Initiative Fellowship.

883

884 **References**

885 1. Mains, P.E., Kemphues, K., Sprunger, S.A., Sulston, I., and Wood, W. (1990).
886 Mutations affecting the meiotic and mitotic divisions of the early Caenorhabditis
887 elegans embryo. Genetics *126*, 593-605.
888 2. McNally, F.J., and Roll-Mecak, A. (2018). Microtubule-severing enzymes: From
889 cellular functions to molecular mechanism. Journal of Cell Biology *217*, 4057-4069.
890 3. Sarbanes, S.L., Zehr, E.A., and Roll-Mecak, A. (2022). Microtubule-severing enzymes.
891 Current Biology *32*, R992-R997.
892 4. Cheung, K., Senese, S., Kuang, J., Bui, N., Ongpipattanakul, C., Gholkar, A., Cohn,
893 W., Capri, J., Whitelegge, J.P., and Torres, J.Z. (2016). Proteomic analysis of the
894 mammalian katanin family of microtubule-severing enzymes defines katanin p80
895 subunit B-like 1 (KATNBL1) as a regulator of mammalian katanin microtubule-
896 severing. Molecular & Cellular Proteomics *15*, 1658-1669.
897 5. Dunleavy, J.E., Okuda, H., O'Connor, A.E., Merriner, D.J., O'Donnell, L., Jamsai, D.,
898 Bergmann, M., and O'Bryan, M.K. (2017). Katanin-like 2 (KATNAL2) functions in
899 multiple aspects of haploid male germ cell development in the mouse. PLOS Genetics
900 *13*, e1007078.
901 6. Sharp, D.J., and Ross, J.L. (2012). Microtubule-severing enzymes at the cutting edge.
902 Journal of Cell Science *125*, 2561-2569. 10.1242/jcs.101139.

903 7. Gomes, J.-E., Tavernier, N., Richaudeau, B., Formstecher, E., Boulin, T., Mains, P.E.,
904 Dumont, J., and Pintard, L. (2013). Microtubule severing by the katanin complex is
905 activated by PPFR-1–dependent MEI-1 dephosphorylation. Journal of Cell Biology
906 *202*, 431-439. 10.1083/jcb.201304174.
907 8. Loughlin, R., Wilbur, J.D., McNally, F.J., Nédélec, F.J., and Heald, R. (2011). Katanin
908 contributes to interspecies spindle length scaling in Xenopus. Cell *147*, 1397-1407.
909 9. Gao, L.L., Xu, F., Jin, Z., Ying, X.Y., and Liu, J.W. (2019). Microtubule-severing
910 protein Katanin p60 ATPase-containing subunit A-like 1 is involved in pole-based
911 spindle organization during mouse oocyte meiosis. Molecular Medicine Reports *20*,
912 3573-3582.
913 10. Lynn, N.A., Martinez, E., Nguyen, H., and Torres, J.Z. (2021). The mammalian family
914 of katanin microtubule-severing enzymes. Frontiers in Cell and Developmental
915 Biology *9*.
916 11. Dunleavy, J.E.M., O'Connor, A.E., Okuda, H., Merriner, D.J., and O'Bryan, M.K.
917 (2021). KATNB1 is a master regulator of multiple katanin enzymes in male meiosis
918 and haploid germ cell development. Development *148*, dev199922.
919 12. O'Donnell, L., Rhodes, D., Smith, S.J., Merriner, D.J., Clark, B.J., Borg, C., Whittle,
920 B., O'Connor, A.E., Smith, L.B., and McNally, F.J. (2012). An essential role for katanin
921 p80 and microtubule severing in male gamete production. PLOS Genetics *8*, e1002698.
922 13. Smith, L.B., Milne, L., Nelson, N., Eddie, S., Brown, P., Atanassova, N., O'Bryan,
923 M.K., O'Donnell, L., Rhodes, D., and Wells, S. (2012). KATNAL1 regulation of Sertoli
924 cell microtubule dynamics is essential for spermiogenesis and male fertility. PLOS
925 Genetics *8*, e1002697.

926 14. Pleuger, C., Lehti, M.S., Dunleavy, J.E., Fietz, D., and O'Bryan, M.K. (2020). Haploid
927 male germ cells—the Grand Central Station of protein transport. Human Reproduction
928 Update *26*, 474-500. 10.1093/humupd/dmaa004.
929 15. Thomas, P.D., Ebert, D., Muruganujan, A., Mushayahama, T., Albou, L.-P., and Mi,
930 H. (2022). PANTHER: Making genome-scale phylogenetics accessible to all. Protein
931 Science *31*, 8-22. https://doi.org/10.1002/pro.4218.
932 16. Liu, L., Zhang, Y., Chang, X., Li, R., Wu, C., Tang, L., and Zhou, Z. (2018).
933 Fluorochloridone perturbs blood-testis barrier/Sertoli cell barrier function through
934 Arp3-mediated F-actin disruption. Toxicology Letters *295*, 277-287.
935 https://doi.org/10.1016/j.toxlet.2018.07.001.
936 17. Lie, P.P., Chan, A.Y., Mruk, D.D., Lee, W.M., and Cheng, C.Y. (2010). Restricted
937 Arp3 expression in the testis prevents blood–testis barrier disruption during junction
938 restructuring at spermatogenesis. Proceedings of the National Academy of Sciences
939 *107*, 11411-11416.
940 18. Li, N., Mruk, D.D., Tang, E.I., Wong, C.K.C., Lee, W.M., Silvestrini, B., and Cheng,
941 C.Y. (2015). Formins: Actin nucleators that regulate cytoskeletal dynamics during
942 spermatogenesis. Spermatogenesis *5*, e1066476. 10.1080/21565562.2015.1066476.
943 19. O'Donnell, L., Nicholls, P.K., O'Bryan, M.K., McLachlan, R.I., and Stanton, P.G.
944 (2011). Spermiation: the process of sperm release. Spermatogenesis *1*, 14-35.
945 20. Takáč, T., Šamajová, O., Pechan, T., Luptovčiak, I., and Šamaj, J. (2017). Feedback
946 microtubule control and microtubule-actin cross-talk in Arabidopsis revealed by
947 integrative proteomic and cell biology analysis of KATANIN 1 mutants. Molecular &
948 Cellular Proteomics *16*, 1591-1609.
949 21. Zhang, D., Grode, K.D., Stewman, S.F., Diaz-Valencia, J.D., Liebling, E., Rath, U.,
950 Riera, T., Currie, J.D., Buster, D.W., Asenjo, A.B., et al. (2011). Drosophila katanin is

951 a microtubule depolymerase that regulates cortical-microtubule plus-end interactions
952 and cell migration. Nature Cell Biology *13*, 361-369. 10.1038/ncb2206.
953 22. Ramalho-Santos, J., Moreno, R.D., Wessel, G.M., Chan, E.K.L., and Schatten, G.
954 (2001). Membrane Trafficking Machinery Components Associated with the
955 Mammalian Acrosome during Spermiogenesis. Experimental Cell Research *267*, 45-
956 60. https://doi.org/10.1006/excr.2000.5119.
957 23. Shan, M.-M., and Sun, S.-C. (2021). The multiple roles of RAB GTPases in female and
958 male meiosis. Human Reproduction Update *27*, 1013-1029.
959 10.1093/humupd/dmab019.
960 24. Blacque, O.E., Scheidel, N., and Kuhns, S. (2018). Rab GTPases in cilium formation
961 and function. Small GTPases *9*, 76-94.
962 25. Lo, J.C., Jamsai, D., O'Connor, A.E., Borg, C., Clark, B.J., Whisstock, J.C., Field,
963 M.C., Adams, V., Ishikawa, T., and Aitken, R.J. (2012). RAB-like 2 has an essential
964 role in male fertility, sperm intra-flagellar transport, and tail assembly.
965 26. Hatakeyama, E., and Hayashi, K. (2018). KATNAL1 is a more active and stable
966 isoform of katanin, and is expressed dominantly in neurons. Biochemical and
967 biophysical research communications *507*, 389-394.
968 27. Rogers, G.C., Rogers, S.L., and Sharp, D.J. (2005). Spindle microtubules in flux.
969 Journal of Cell Science *118*, 1105-1116.
970 28. Rath, U., and Sharp, D.J. (2011). The molecular basis of anaphase A in animal cells.
971 Chromosome Research *19*, 423-432. 10.1007/s10577-011-9199-2.
972 29. Jiang, K., Rezabkova, L., Hua, S., Liu, Q., Capitani, G., Altelaar, A., Heck, A.J.,
973 Kammerer, R.A., Steinmetz, M.O., and Akhmanova, A. (2017). Microtubule minus-
974 end regulation at spindle poles by an ASPM–katanin complex. Nature cell biology *19*,
975 480-492.

976 30. Zhang, D., Rogers, G.C., Buster, D.W., and Sharp, D.J. (2007). Three microtubule
977 severing enzymes contribute to the "Pacman-flux" machinery that moves
978 chromosomes. The Journal of cell biology *177*, 231-242.
979 31. Elad, N., Abramovitch, S., Sabanay, H., and Medalia, O. (2011). Microtubule
980 organization in the final stages of cytokinesis as revealed by cryo-electron tomography.
981 Journal of Cell Science *124*, 207-215. 10.1242/jcs.073486.
982 32. Cheers, S.R., O'Connor, A.E., Johnson, T.K., Merriner, D.J., O'Bryan, M.K., and
983 Dunleavy, J.E. (2022). Spastin is an essential regulator of male meiosis, acrosome
984 formation, manchette structure and nuclear integrity. bioRxiv.
985 33. Lehti, M., and Sironen, A. (2016). Formation and function of the manchette and
986 flagellum during spermatogenesis. Reproduction *151*, R43-54.
987 34. Cotton, L.M., Meilak, M.L., Templeton, T., Gonzales, J.G., Nenci, A., Cooney, M.,
988 Truman, D., Rodda, F., Lynas, A., and Viney, E. (2015). Utilising the resources of the
989 International Knockout Mouse Consortium: the Australian experience. Mammalian
990 Genome *26*, 142-153.
991 35. Sadate-Ngatchou, P.I., Payne, C.J., Dearth, A.T., and Braun, R.E. (2008). Cre
992 recombinase activity specific to postnatal, premeiotic male germ cells in transgenic
993 mice. Genesis *46*, 738-742.
994 36. Dunleavy, J.E.M., O'Connor, A.E., and O'Bryan, M.K. (2019). An optimised STAPUT
995 method for the purification of mouse spermatocyte and spermatid populations.
996 Molecular Human Reproduction *25*, 675-683. 10.1093/molehr/gaz056.
997 37. Livak, K.J., and Schmittgen, T.D. (2001). Analysis of Relative Gene Expression Data
998 Using Real-Time Quantitative PCR and the $2^{-\Delta\Delta CT}$ Method. Methods *25*, 402-408.

999 38. Houston, B.J., Conrad, D.F., and O'Bryan, M.K. (2020). A framework for high-
1000 resolution phenotyping of candidate male infertility mutants: from human to mouse.
1001 Human Genetics, 1-28.
1002 39. Cotton, L., Gibbs, G.M., Sanchez-Partida, L.G., Morrison, J.R., de Kretser, D.M., and
1003 O'Bryan, M.K. (2006). FGFR-1 signaling is involved in spermiogenesis and sperm
1004 capacitation. Journal of Cell Science *119*, 75-84.
1005 40. Baker, M.A., Hetherington, L., Weinberg, A., and Velkov, T. (2014). Phosphopeptide
1006 analysis of rodent epididymal spermatozoa. JoVE (Journal of Visualized Experiments),
1007 e51546.
1008 41. Gibbs, G.M., Orta, G., Reddy, T., Koppers, A.J., Martínez-López, P., Luis de la Vega-
1009 Beltran, J., Lo, J.C., Veldhuis, N., Jamsai, D., and McIntyre, P. (2011). Cysteine-rich
1010 secretory protein 4 is an inhibitor of transient receptor potential M8 with a role in
1011 establishing sperm function. Proceedings of the National Academy of Sciences *108*,
1012 7034-7039.
1013 42. O'Bryan, M.K., Clark, B.J., McLaughlin, E.A., D'Sylva, R.J., O'Donnell, L., Wilce,
1014 J.A., Sutherland, J., O'Connor, A.E., Whittle, B., and Goodnow, C.C. (2013). RBM5 is
1015 a male germ cell splicing factor and is required for spermatid differentiation and male
1016 fertility. PLoS genetics *9*, e1003628.
1017 43. Gibbs, G.M., Lo, J.C.Y., Nixon, B., Jamsai, D., O'Connor, A.E., Rijal, S., Sanchez-
1018 Partida, L.G., Hearn, M.T.W., Bianco, D.M., and O'Bryan, M.K. (2010). Glioma
1019 Pathogenesis-Related 1-Like 1 Is Testis Enriched, Dynamically Modified, and
1020 Redistributed during Male Germ Cell Maturation and Has a Potential Role in Sperm-
1021 Oocyte Binding. Endocrinology *151*, 2331-2342. 10.1210/en.2009-1255.
1022 44. Jamsai, D., Bianco, D.M., Smith, S.J., Merriner, D.J., Ly-Huynh, J.D., Herlihy, A.,
1023 Niranjan, B., Gibbs, G.M., and O'Bryan, M.K. (2008). Characterization of

1024 gametogenetin 1 (GGN1) and its potential role in male fertility through the interaction
1025 with the ion channel regulator, cysteine-rich secretory protein 2 (CRISP2) in the sperm
1026 tail. Reproduction *135*, 751-760.
1027 45. R Core Development Team (2015). R: A language and environment for statistical
1028 computing. R Foundation for Statistical Computing.
1029 46. Bates, D., Mächler, M., Bolker, B., and Walker, S. (2015). Fitting Linear Mixed-Effects
1030 Models Using lme4. Journal of Statistical Software *67*. 10.18637/jss.v067.i01.
1031 47. Brooks, M.E., Kristensen, K., van Benthem, K.J., Magnusson, A., Berg, C.W., Nielsen,
1032 A., Skaug, H.J., Machler, M., and Bolker, B.M. (2017). glmmTMB balances speed and
1033 flexibility among packages for zero-inflated generalized linear mixed modeling. The R
1034 Journal *9*, 378-400.
1035 48. Lin, Y.-H., Huang, C.-Y., Ke, C.-C., Wang, Y.-Y., Lai, T.-H., Liu, H.-C., Ku, W.-C.,
1036 Chan, C.-C., and Lin, Y.-H. (2020). ACTN4 mediates SEPT14 mutation-induced sperm
1037 head defects. Biomedicines *8*, 518.
1038 49. Hsu, W.H., Wang, W.J., Lin, W.Y., Huang, Y.M., Lai, C.C., Liao, J.C., and Chen, H.C.
1039 (2018). Adducin-1 is essential for spindle pole integrity through its interaction with
1040 TPX2. EMBO Rep *19*. 10.15252/embr.201745607.
1041 50. Chan, P.C., Hsu, R.Y., Liu, C.W., Lai, C.C., and Chen, H.C. (2014). Adducin-1 is
1042 essential for mitotic spindle assembly through its interaction with myosin-X. J Cell Biol
1043 *204*, 19-28. 10.1083/jcb.201306083.
1044 51. Adams, M., Simms, R.J., Abdelhamed, Z., Dawe, H.R., Szymanska, K., Logan, C.V.,
1045 Wheway, G., Pitt, E., Gull, K., Knowles, M.A., et al. (2012). A meckelin-filamin A
1046 interaction mediates ciliogenesis. Hum Mol Genet *21*, 1272-1286.
1047 10.1093/hmg/ddr557.

1048 52. Yuan, S., Stratton, C.J., Bao, J., Zheng, H., Bhetwal, B.P., Yanagimachi, R., and Yan,
1049 W. (2015). Spata6 is required for normal assembly of the sperm connecting piece and
1050 tight head-tail conjunction. Proc Natl Acad Sci U S A *112*, E430-439.
1051 10.1073/pnas.1424648112.
1052 53. Sangokoya, C., and Blelloch, R. (2020). MicroRNA-dependent inhibition of PFN2
1053 orchestrates ERK activation and pluripotent state transitions by regulating endocytosis.
1054 Proc Natl Acad Sci U S A *117*, 20625-20635. 10.1073/pnas.2002750117.
1055 54. Lee, N.P.Y., Mruk, D.D., Conway, A.M., and Cheng, C.Y. (2004). Zyxin, Axin, and
1056 Wiskott-Aldrich Syndrome Protein Are Adaptors That Link the Cadherin/Catenin
1057 Protein Complex to the Cytoskeleton at Adherens Junctions in the Seminiferous
1058 Epithelium of the Rat Testis. Journal of Andrology *25*, 200-215.
1059 https://doi.org/10.1002/j.1939-4640.2004.tb02780.x.
1060 55. Qi, Y., Jiang, M., Yuan, Y., Bi, Y., Zheng, B., Guo, X., Huang, X., Zhou, Z., and Sha,
1061 J. (2013). ADP-ribosylation factor-like 3, a manchette-associated protein, is essential
1062 for mouse spermiogenesis. Molecular Human Reproduction *19*, 327-335.
1063 10.1093/molehr/gat001.
1064 56. Barbosa, D.J., Teixeira, V., Duro, J., Carvalho, A.X., and Gassmann, R. (2021).
1065 Dynein-dynactin segregate meiotic chromosomes in C. elegans spermatocytes.
1066 Development *148*. 10.1242/dev.197780.
1067 57. Wu, C.-H., Zong, Q., Du, A.-L., Zhang, W., Yao, H.-C., Yu, X.-Q., and Wang, Y.-F.
1068 (2016). Knockdown of Dynamitin in testes significantly decreased male fertility in
1069 Drosophila melanogaster. Developmental biology *420*, 79-89.
1070 58. Fouquet, J., Kann, M., Soues, S., and Melki, R. (2000). ARP1 in Golgi organisation
1071 and attachment of manchette microtubules to the nucleus during mammalian
1072 spermatogenesis. Journal of Cell Science *113*, 877-886. 10.1242/jcs.113.5.877.

1073 59. Tarkar, A., Loges, N.T., Slagle, C.E., Francis, R., Dougherty, G.W., Tamayo, J.V.,
1074 Shook, B., Cantino, M., Schwartz, D., Jahnke, C., et al. (2013). DYX1C1 is required
1075 for axonemal dynein assembly and ciliary motility. Nature Genetics *45*, 995-1003.
1076 10.1038/ng.2707.
1077 60. Tang, E.I., Mok, K.W., Lee, W.M., and Cheng, C.Y. (2015). EB1 regulates tubulin and
1078 actin cytoskeletal networks at the sertoli cell blood-testis barrier in male rats: an in vitro
1079 study. Endocrinology *156*, 680-693. 10.1210/en.2014-1720.
1080 61. Wang, F., Zhang, Q., Cao, J., Huang, Q., and Zhu, X. (2008). The microtubule plus
1081 end-binding protein EB1 is involved in Sertoli cell plasticity in testicular seminiferous
1082 tubules. Experimental Cell Research *314*, 213-226.
1083 https://doi.org/10.1016/j.yexcr.2007.09.022.
1084 62. Kanemori, Y., Koga, Y., Sudo, M., Kang, W., Kashiwabara, S.-i., Ikawa, M., Hasuwa,
1085 H., Nagashima, K., Ishikawa, Y., and Ogonuki, N. (2016). Biogenesis of sperm
1086 acrosome is regulated by pre-mRNA alternative splicing of Acrbp in the mouse.
1087 Proceedings of the National Academy of Sciences *113*, E3696-E3705.
1088 63. Selvaraj, V., Asano, A., Page, J.L., Nelson, J.L., Kothapalli, K.S.D., Foster, J.A.,
1089 Brenna, J.T., Weiss, R.S., and Travis, A.J. (2010). Mice lacking FABP9/PERF15
1090 develop sperm head abnormalities but are fertile. Developmental Biology *348*, 177-
1091 189. https://doi.org/10.1016/j.ydbio.2010.09.019.
1092 64. Dix, D.J., Allen, J.W., Collins, B.W., Mori, C., Nakamura, N., Poorman-Allen, P.,
1093 Goulding, E.H., and Eddy, E.M. (1996). Targeted gene disruption of Hsp70-2 results
1094 in failed meiosis, germ cell apoptosis, and male infertility. Proceedings of the National
1095 Academy of Sciences *93*, 3264-3268. doi:10.1073/pnas.93.8.3264.
1096 65. Dix, D.J., Allen, J.W., Collins, B.W., Poorman-Allen, P., Mori, C., Blizard, D.R.,
1097 Brown, P.R., Goulding, E.H., Strong, B.D., and Eddy, E.M. (1997). HSP70-2 is

1098 required for desynapsis of synaptonemal complexes during meiotic prophase in
1099 juvenile and adult mouse spermatocytes. Development *124*, 4595-4603.
1100 10.1242/dev.124.22.4595.
1101 66. Govin, J., Caron, C., Escoffier, E., Ferro, M., Kuhn, L., Rousseaux, S., Eddy, E.M.,
1102 Garin, J., and Khochbin, S. (2006). Post-meiotic shifts in HSPA2/HSP70.2 chaperone
1103 activity during mouse spermatogenesis. J Biol Chem *281*, 37888-37892.
1104 10.1074/jbc.M608147200.
1105 67. Yang , F., Eckardt , S., Leu , N.A., McLaughlin , K.J., and Wang , P.J. (2008). Mouse
1106 TEX15 is essential for DNA double-strand break repair and chromosomal synapsis
1107 during male meiosis. Journal of Cell Biology *180*, 673-679. 10.1083/jcb.200709057.
1108 68. Schöpp, T., Zoch, A., Berrens, R.V., Auchynnikava, T., Kabayama, Y., Vasiliauskaitė,
1109 L., Rappsilber, J., Allshire, R.C., and O'Carroll, D. (2020). TEX15 is an essential
1110 executor of MIWI2-directed transposon DNA methylation and silencing. Nature
1111 Communications *11*, 3739. 10.1038/s41467-020-17372-5.
1112 69. Mountjoy, J.R., Xu, W., McLeod, D., Hyndman, D., and Oko, R. (2008). RAB2A: a
1113 major subacrosomal protein of bovine spermatozoa implicated in acrosomal biogenesis.
1114 Biol Reprod *79*, 223-232. 10.1095/biolreprod.107.065060.
1115 70. Morohoshi, A., Miyata, H., Oyama, Y., Oura, S., Noda, T., and Ikawa, M. (2021).
1116 FAM71F1 binds to RAB2A and RAB2B and is essential for acrosome formation and
1117 male fertility in mice. Development *148*. 10.1242/dev.199644.
1118 71. Da Costa, R., Bordessoules, M., Guilleman, M., Carmignac, V., Lhussiez, V., Courot,
1119 H., Bataille, A., Chlémaire, A., Bruno, C., Fauque, P., et al. (2020). Vps13b is required
1120 for acrosome biogenesis through functions in Golgi dynamic and membrane trafficking.
1121 Cellular and Molecular Life Sciences *77*, 511-529. 10.1007/s00018-019-03192-4.
1122

1123 **Figures**

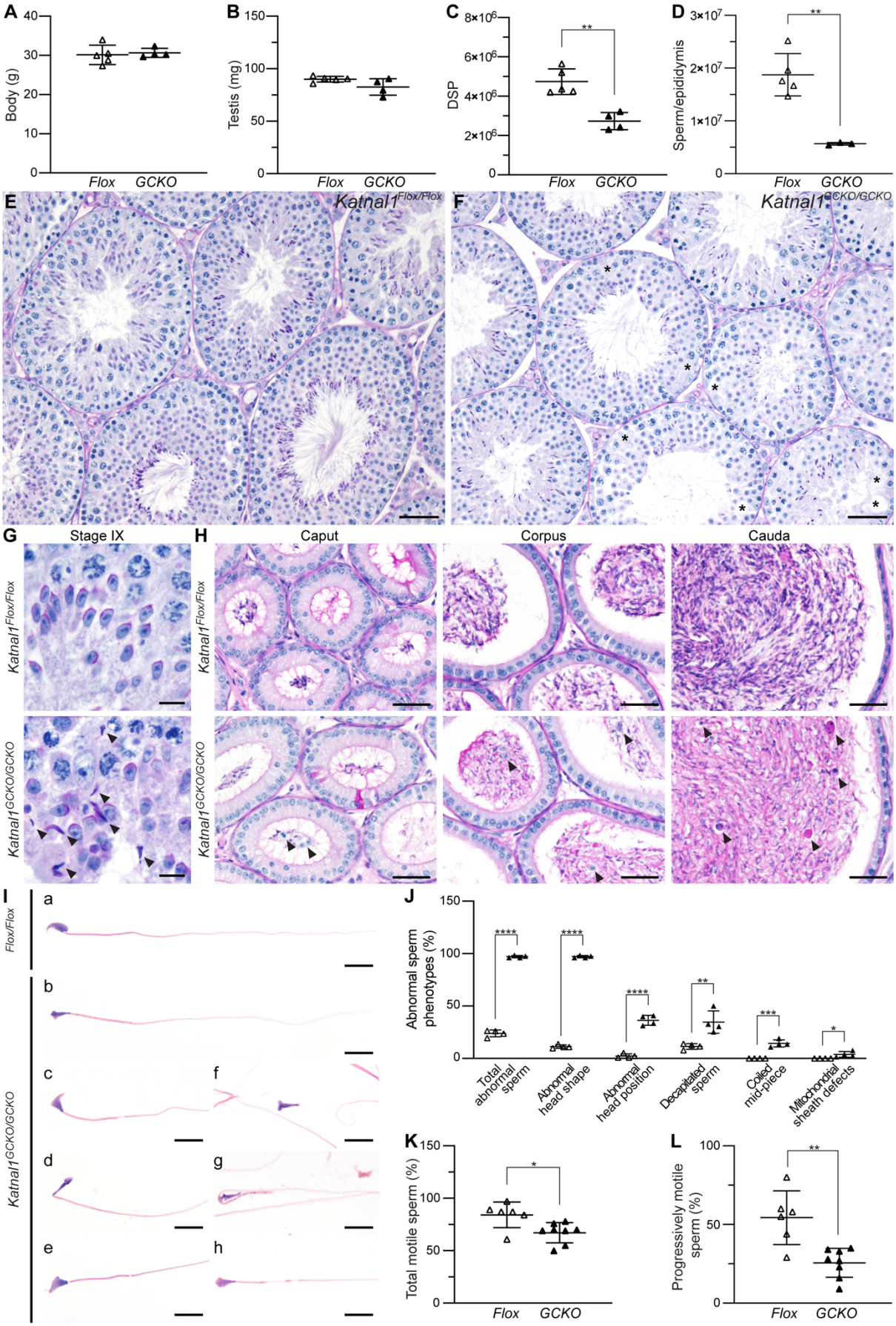

1124

1125 **Figure 1: Germ cell derived KATNAL1 is required for optimal male fertility**

1126 Body weight (**A**), testis weight (**B**), DSP (**C**), and epididymal sperm content (**D**) in
1127 *Katnal1*$^{GCKO/GCKO}$ mice (black triangles) and *Katnal1*$^{Flox/Flox}$ controls (white triangles)
1128 (n≥3/genotype). Lines represent mean ± SD. PAS-stained testis (**E-G**) and epididymis (**H**)
1129 sections. Asterisks indicate areas of seminiferous epithelium with vacuoles or devoid of germ
1130 cells. Black arrowheads indicate retained spermatids. (**I)** Hematoxylin and eosin-stained cauda
1131 epididymal sperm. Abnormalities were observed in the vast majority of sperm from
1132 *Katnal1*$^{GCKO/GCKO}$ mice. Defects included abnormal sperm head shapes - "knobby" (b) and
1133 "hammer" head (c, f), abnormal head sperm head position (d), decapitated sperm (e,), coiled
1134 mid-pieces (g) and occasionally, mitochondrial sheath defects (h). (**J**) Quantification of
1135 abnormal cauda epididymal sperm phenotypes in *Katnal1*$^{Flox/Flox}$ (white triangles) versus
1136 *Katnal1*$^{GCKO/GCKO}$ (black triangles). (n≥3/genotype). Percentage of motile sperm (**K**) and
1137 percentage of progressively motile sperm (**L**) from *Katnal1*$^{Flox/Flox}$ (white triangles) versus
1138 *Katnal1*$^{GCKO/GCKO}$ (black triangles) males. Scale bars in **E-F** = 50 μm**, G** = 10 μm, **H** = 40 μm,
1139 **I** = 10 μm. **P*<0.05 , ***P*<0.01, ****P*<0.01, *****P*<0.001.

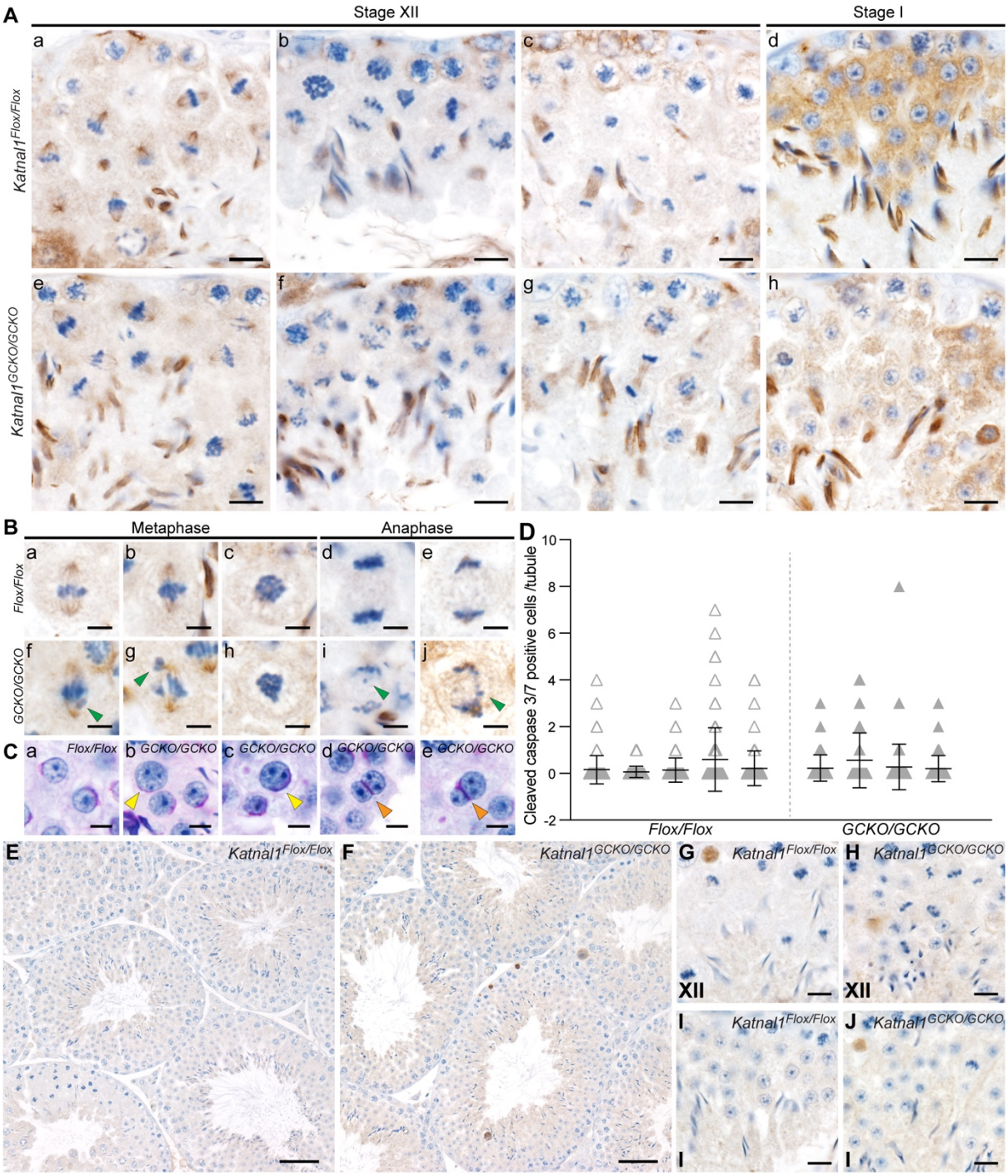

Figure 2: KATNAL1 regulates chromosome alignment, segregation and cytokinesis during male meiosis

(**A-B**) Seminiferous tubule sections immunolabelled for α-tubulin as a component of MTs. Nuclei are counterstained with hematoxylin. Green arrowheads indicate misaligned/lagging chromosomes. (**C**) PAS-stained testis sections showing abnormally large round spermatid nuclei (b,c; yellow arrowhead) and binucleated round spermatids (d-e; orange arrowheads) in

1147 *Katnal1*$^{GCKO/GCKO}$ mice. (**D-J**) Germ cell apoptosis in *Katnal1*$^{GCKO/GCKO}$ mice was assessed by
1148 immunolabelling of seminiferous tubules for cleaved-caspase 3 and 7. The average number of
1149 cleaved-caspase 3 and/or 7 positive germ cells per seminiferous tubule is graphed in **D** and
1150 representative images are shown in **E-G**. In **D** lines represent mean ±SD. A minimum of 80
1151 randomly selected tubules per mouse were counted (n≥3/genotype). Scale bars in **A**-**B**,**G-J** =
1152 10 μm**, C**=5 μm**. E**-**F**= 50 μm.
1153

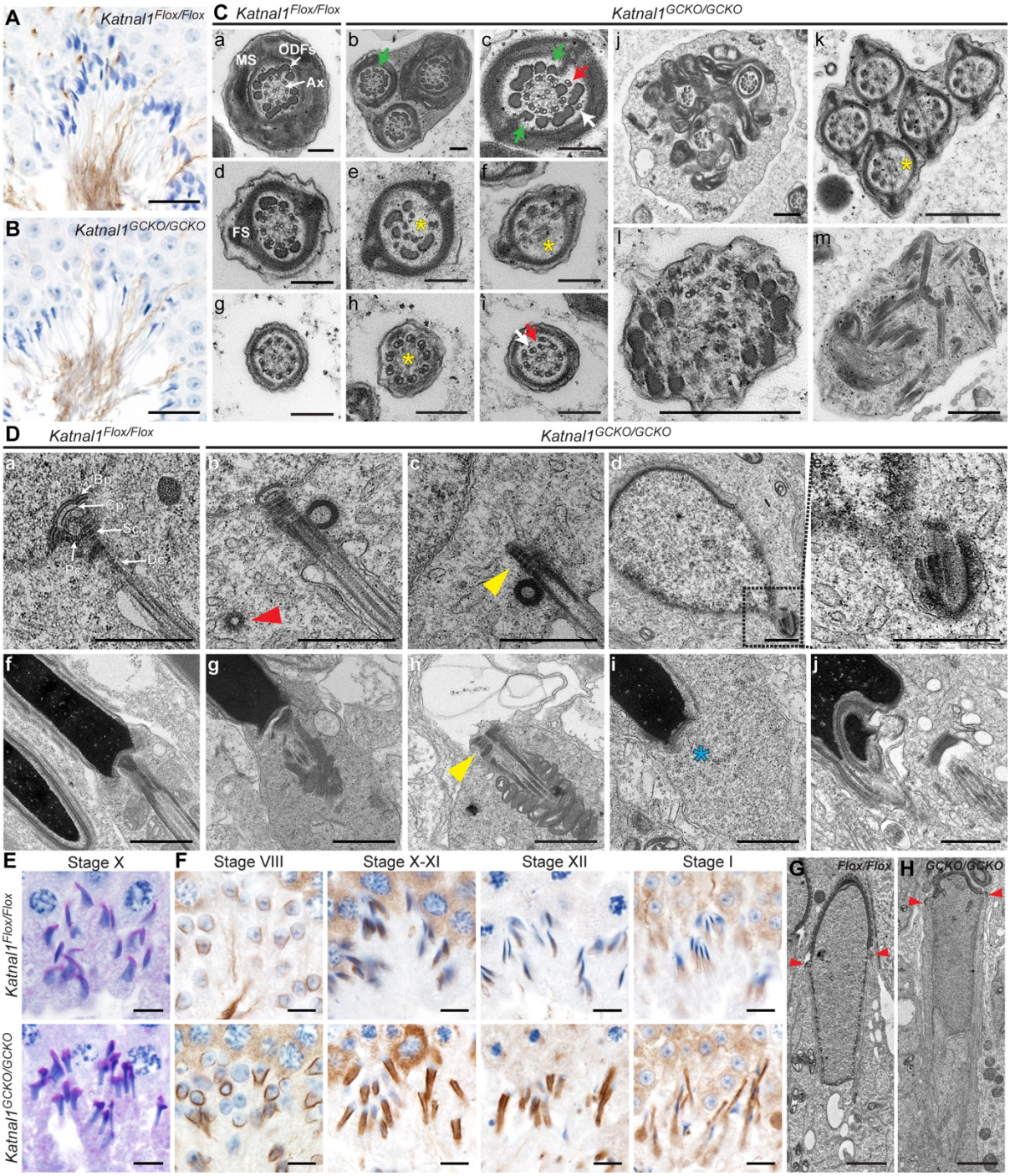

Figure 3: KATNAL1 is a regulator of flagella formation and the MT manchette in male germ cells

Testis sections immunolabelled for the axoneme marker acetylated tubulin in *Katnal1*$^{Flox/Flox}$ (**A**) and *Katnal1*$^{GCKO/GCKO}$ (**B**). (**C**) TEM of flagella ultrastructure in cauda epididymal sperm of *Katnal1*$^{Flox/Flox}$ and *Katnal1*$^{GCKO/GCKO}$ mice. MS= mitochondrial sheath, ODFs = outer dense fibers, Ax=axoneme FS = fibrous sheath. White arrows indicate supernumerary MT doublets.

1161 Red arrows indicate ectopic MT doublets. Green arrows indicate ectopic ODFs. Yellow
1162 asterisks indicate missing axoneme MT doublets/or central pair. (**D**) TEM of HTCA
1163 ultrastructure in round (**a-e**) and elongated spermatids (**f-j**) in *Katnal1*$^{Flox/Flox}$ and
1164 *Katnal1*$^{GCKO/GCKO}$ mice. Red arrowhead indicated supernumerary centriole. Blue asterisks
1165 indicate absent HTCA. Yellow arrowheads indicate HTCAs are abnormally detached from the
1166 nucleus. (**E**) PAS-stained testis sections showing *Katnal1*$^{Flox/Flox}$ and *Katnal1*$^{GCKO/GCKO}$
1167 elongating spermatids. (**F**) Testis sections immunolabelled for α-tubulin as a maker of the
1168 manchette in *Katnal1*$^{Flox/Flox}$ and *Katnal1*$^{GCKO/GCKO}$ mice. Progressive steps of manchette
1169 formation, migration and dissolution are shown left to right. **(G-H)** TEM showing manchette
1170 structure in *Katnal1*$^{Flox/Flox}$ and *Katnal1*$^{GCKO/GCKO}$ elongating spermatids. Red arrowheads
1171 indicate the perinuclear ring. Scale bars in **A-B** = 20 μm**, Ca-i =** 200 nm, **Cj-m** = 500 nm, **D** =
1172 1 μm, **E-F**=10 μm, **G-H** = 2 μm**.**

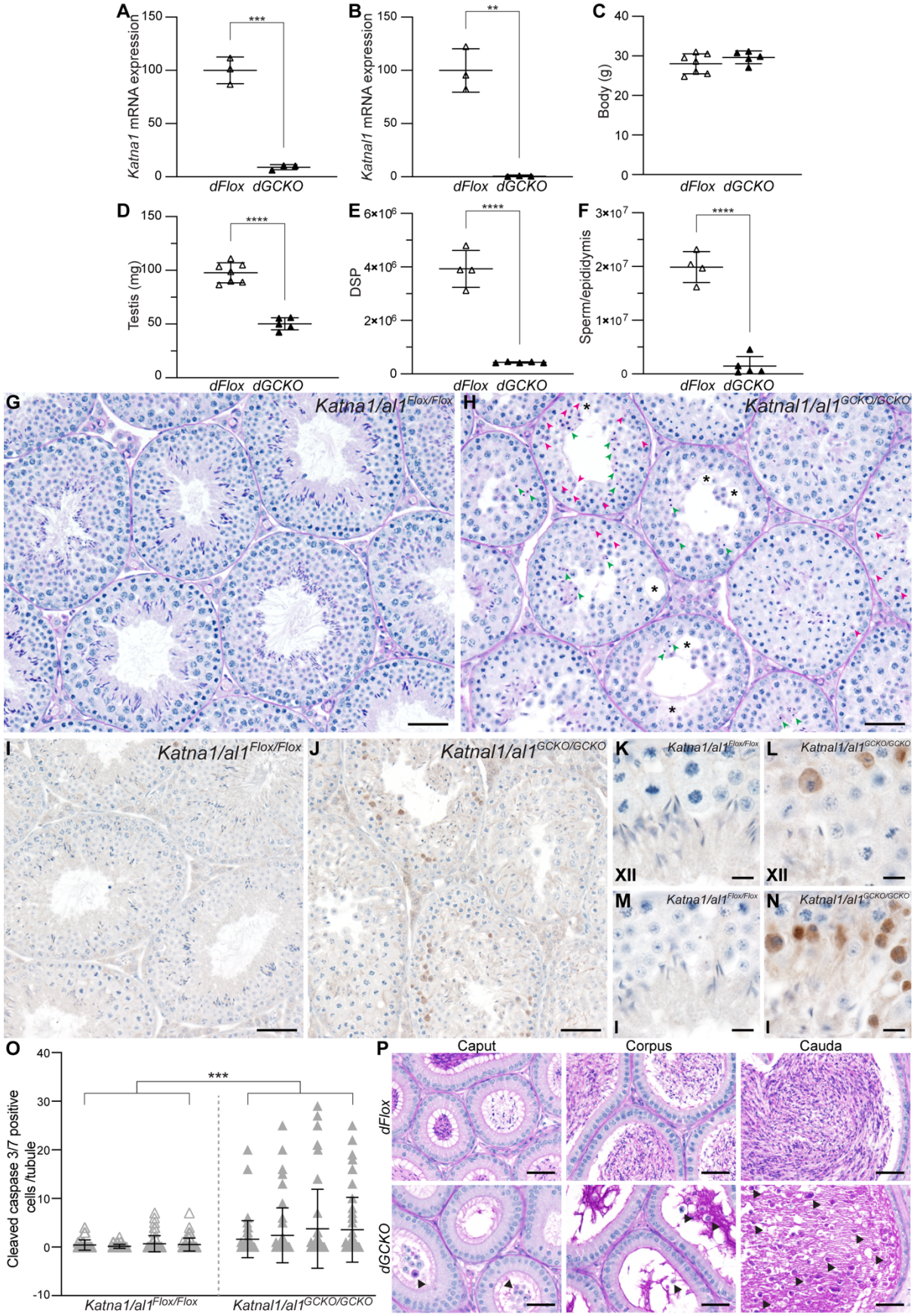
A
Katna1 mRNA expression
150
100
50
0
***
dFlox dGCKO
B
Katnal1 mRNA expression
150
100
50
0
**
dFlox dGCKO
C
Body (g)
40
30
20
10
0
dFlox dGCKO
D
Testis (mg)
150
100
50
0
****
dFlox dGCKO
E
DSP
6×10^6
4×10^6
2×10^6
0
****
dFlox dGCKO
F
Sperm/epididymis
3×10^7
2×10^7
1×10^7
0
****
dFlox dGCKO
G
Katna1/al1^Flox/Flox
H
Katnal1/al1^GCKO/GCKO
I
Katna1/al1^Flox/Flox
J
Katnal1/al1^GCKO/GCKO
K
Katna1/al1^Flox/Flox
XII
L
Katnal1/al1^GCKO/GCKO
XII
M
Katna1/al1^Flox/Flox
I
N
Katnal1/al1^GCKO/GCKO
I
O
Cleaved caspase 3/7 positive cells /tubule
40
30
20
10
0
-10
***
Katna1/al1^Flox/Flox
Katnal1/al1^GCKO/GCKO
P
Caput
Corpus
Cauda
dFlox
dGCKO

1173

1174 **Figure 4: Double germ cell deletion of KATNA1 and KATNAL1 results in a severe**
1175 **oligozoospermia-like phenotype**

1176 qPCR analysis of *Katna1* (**A**) and *Katnal1* (**B**) transcript levels in *Katna1/al1*$^{GCKO/GCKO}$ (black
1177 triangles, *dGCKO*) isolated spermatocytes relative to *Katna1/al1*$^{Flox/Flox}$ (white triangles,
1178 *dFlox*) isolated spermatocytes (n≥3/genotype). Body weight (**C**), testis weight (**D**), testis DSP
1179 (**E**), and epididymal sperm content (**F**) in *Katna1/al1*$^{GCKO/GCKO}$ (black triangles) compared to
1180 *Katna1/al1*$^{Flox/Flox}$ controls (white triangles) (n≥3/genotype). Lines represent mean ± SD. PAS-
1181 stained testis (**G-H**) sections from *Katna1/al1*$^{GCKO/GCKO}$ and *Katna1/al1*$^{Flox/Flox}$ mice. Magenta
1182 arrowheads indicate pyknotic spermatocytes and green arrowheads indicate pyknotic
1183 spermatids. Asterisks indicate areas of seminiferous epithelium with vacuoles or devoid of
1184 germ cells. Analysis of germ cell apoptosis in *Katnal1*$^{GCKO/GCKO}$ mice relative to
1185 *Katna1/al1*$^{Flox/Flox}$ mice (**I-O**). Representative images of testis immunolabelling of cleaved-
1186 caspase 3 and 7 are shown in (**I-N**). Roman numerals denote seminiferous tubule stage. The
1187 average number of cleaved-caspase 3 and/or 7 positive germ cells per seminiferous tubule per
1188 mouse is graphed in (**O**). In **O** lines represent mean ±SD. A minimum of 50 randomly selected
1189 tubules per mouse were counted (n≥3/genotype). PAS-stained epididymis sections (**P**) from
1190 *Katna1/al1*$^{GCKO/GCKO}$ and *Katna1/al1*$^{Flox/Flox}$ mice. Scale bars in **G-J** = 50 µm, in **K-N** = 10 µm,
1191 **P** = 40 µm. **P*<0.05 , ***P*<0.01, ****P*<0.01, *****P*<0.001.

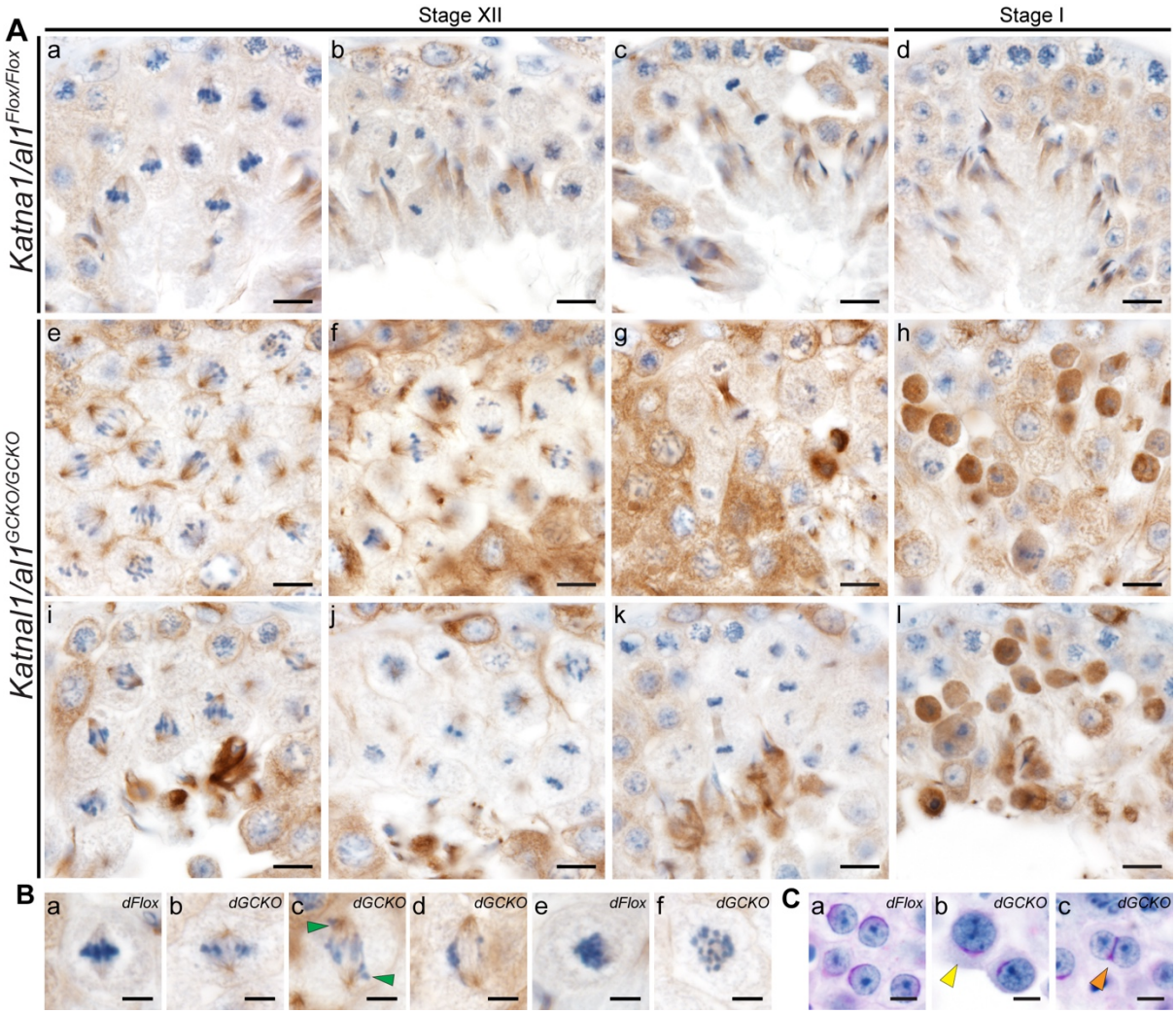

1192

1193 **Figure 5: KATNA1 and KATNAL1 compensate for each other in male meiosis**

1194 (**A-B**) *Katnal1/al1*$^{Flox/Flox}$ (*dFlox*) and *Katna1/al1*$^{GCKO/GCKO}$ (*dGCKO*) seminiferous tubule

1195 sections immunolabelled for MTs (α-tubulin). Nuclei are counterstained with hematoxylin.

1196 Green arrowheads indicate misaligned/lagging chromosomes. (**C**) PAS-stained

1197 *Katnal1/al1*$^{Flox/Flox}$ (*dFlox*) and *Katna1/al1*$^{GCKO/GCKO}$ (*dGCKO*) testis sections showing

1198 abnormally large round spermatid nuclei (b; yellow arrowhead) and binucleated round

1199 spermatids (c; orange arrowheads) in *Katna1/al1*$^{GCKO/GCKO}$ mice. Scale bars in **A**= 10 µm, in

1200 **B-C**= 5 µm.

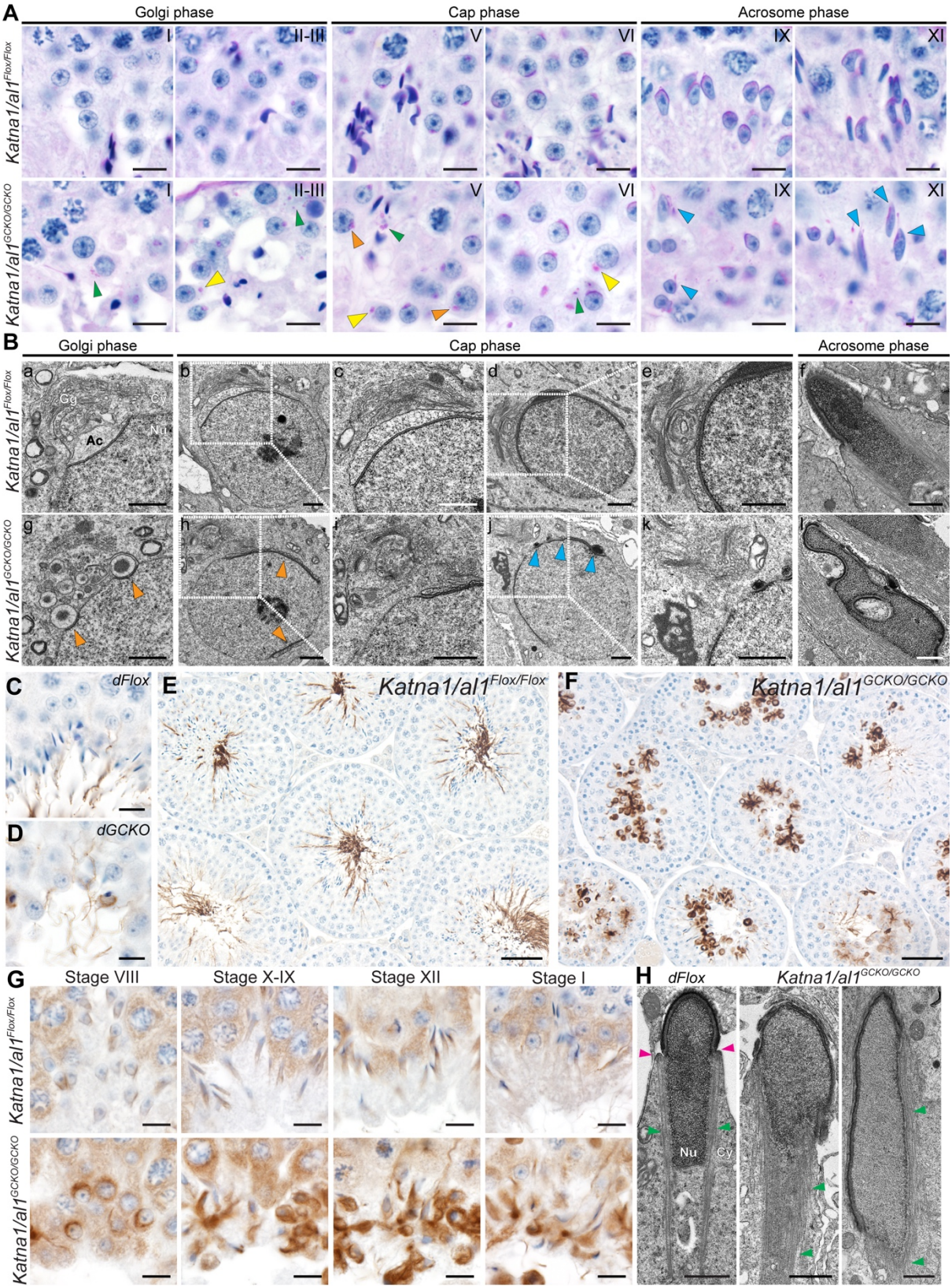

Figure 6: **KATNA1 and KATNAL1 compensation in spermatid acrosome formation and MT regulation**

1204 (**A**) PAS-stained testis sections showing acrosome formation in *Katna1/al1*$^{Flox/Flox}$ and
1205 *Katna1/al1*$^{GCKO/GCKO}$ mice. Progressive steps of acrosome formation are shown left to right.
1206 Roman numerals denote seminiferous tubule stage. Orange arrowheads indicate nuclei with
1207 more than one proacrosomal vesicle attached. Yellow arrowheads indicate acrosomal vesicles
1208 not attached to the nucleus. Green arrowheads indicate ectopic PAS positive vesicles
1209 abnormally dispersed in round spermatid cytoplasm. Blue arrowheads indicate elongating
1210 spermatids with abnormal gaps/fragmentation of the acrosomes. (**B**) Electron micrographs
1211 showing acrosome and Golgi apparatus ultrastructure in *Katna1/al1*$^{Flox/Flox}$ and
1212 *Katna1/al1*$^{GCKO/GCKO}$ mice. Orange arrowheads indicate supernumerary site of acrosome
1213 formation. Blue arrowheads indicate numerous small unfused acrosomal vesicles docked at the
1214 nuclear membrane/fragmentation of the acrosome. (**C-F**) *Katna1/al1*$^{Flox/Flox}$ (*dFlox*) and
1215 *Katna1/al1*$^{GCKO/GCKO}$ (*dGCKO*) mouse testis sections immunolabelled for the sperm tails
1216 marker acetylated tubulin. (**G**) *Katna1/al1*$^{Flox/Flox}$ and *Katna1/al1*$^{GCKO/GCKO}$ testis sections
1217 immunolabelled for α-tubulin as a maker of the manchette. Progressive steps of manchette
1218 formation, migration and dissolution are shown left to right. TEM showing nuclear and
1219 manchette morphology in *Katna1/al1*$^{Flox/Flox}$ (*dFlox*) and *Katnal1*$^{GCKO/GCKO}$ mouse elongating
1220 spermatids. Red arrowheads indicate the perinuclear ring. Blue arrowheads indicate MTs. Scale
1221 bars in **A, C-D** = 10 µm, **B,H** = 1 µm, **E-F** = 50 µm, **G**=10 µm. Nu = Nucleus, Cy =cytoplasm
1222 Gg=Golgi apparatus, Ac=acrosome.

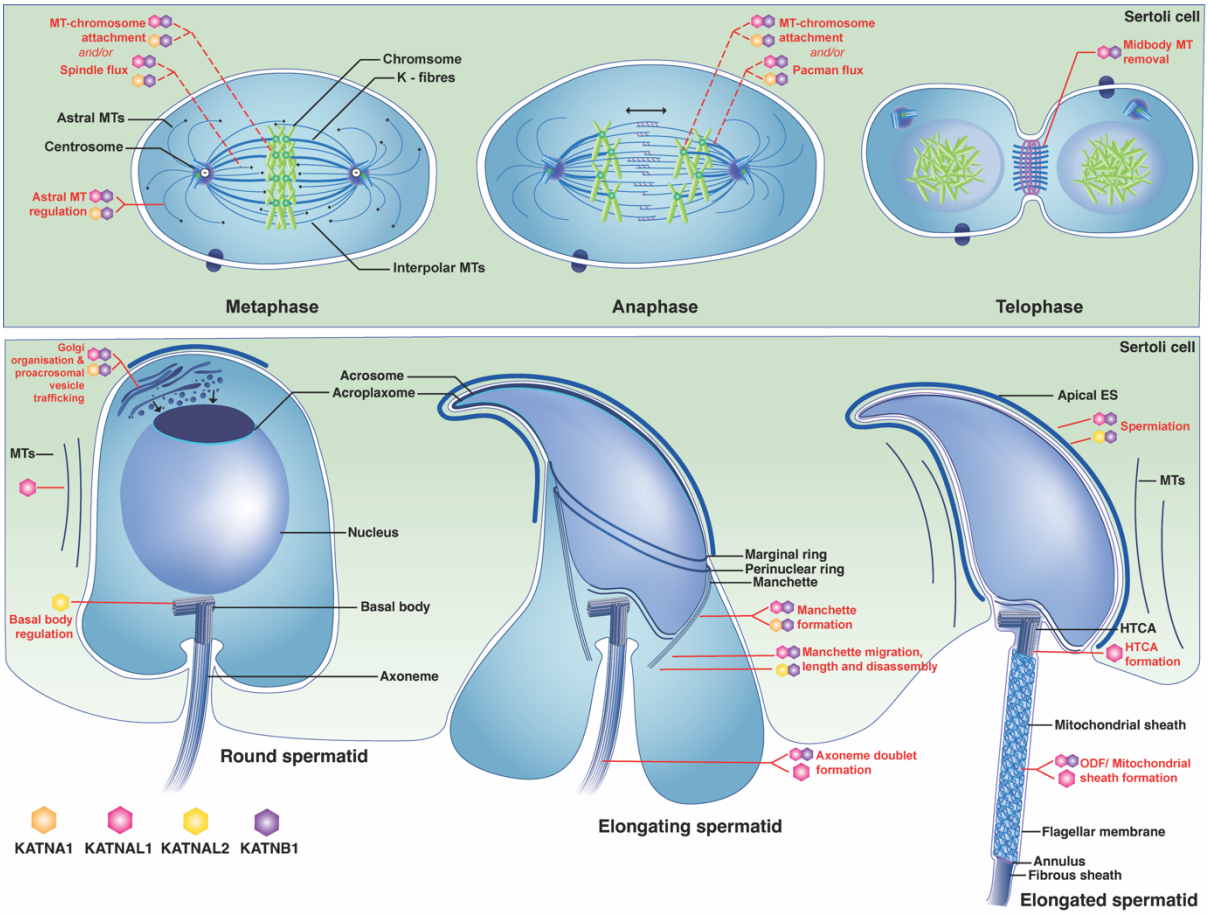

Figure 7: Proposed model of katanin regulation of spermatogenesis

KATNB1-independent and -dependent functions of each katanin A-subunit during male germ cell development are depicted based on the data defined herein and defined for KATNAL1 Sertoli cell function in [13], for KATNAL2 in [5] and KATNB1 defined in [11,12]. A shared line indicates two complexes have redundant/compensatory function in the process indicated. HTCA = head to tail coupling apparatus, MTs = microtubule, ODF = outer dense fibers.